Port-Hamiltonian formulation and
Symplectic discretization of Plate models
Part I : Mindlin model for thick plates

Andrea Brugnoli[a,*], Daniel Alazard[a], Valérie Pommier-Budinger[a], Denis Matignon[a]

[a]*ISAE-SUPAERO, Université de Toulouse, France.*

10 Avenue Edouard Belin, BP-54032, 31055 Toulouse Cedex 4.

Abstract

The port-Hamiltonian formulation is a powerful method for modeling and interconnecting systems of different natures. In this paper, the port-Hamiltonian formulation in tensorial form of a thick plate described by the Mindlin-Reissner model is presented. Boundary control and observation are taken into account. Thanks to tensorial calculus, it can be seen that the Mindlin plate model mimics the interconnection structure of its one-dimensional counterpart, i.e. the Timoshenko beam.

The Partitioned Finite Element Method (PFEM[1]) is then extended to both the vectorial and tensorial formulations in order to obtain a suitable, i.e. structure-preserving, finite-dimensional port-Hamiltonian system (PHs[2]), which preserves the structure and properties of the original distributed parameter system. Mixed boundary conditions are finally handled by introducing some algebraic constraints.

Numerical examples are finally presented to validate this approach.

Keywords: Port-Hamiltonian systems, Mindlin-Reissner plate, Partitioned Finite Element Method, geometric spatial discretization, boundary control.

Introduction

The port-Hamiltonian (PH) framework is acquiring more visibility for its capability to represent a huge class of systems coming from different realms of physics. The Hamiltonian formalism arising from the Legendre transformation of Euler-Lagrange system has been already widely explored [1]. This approach offer insights on analytical solutions (see [2] for a closed solution of the eigen problem of rectangular Reissner plates) and is of use whenever easy engineering solutions are sought after. The Legendre transformation gives rise to a system of equations ruled by a Hamiltonian matrix on a symplectic space. On the contrary, PH systems are defined with respect to a Hamiltonian operator [3, Chapter 7]. For a detailed

---

*Corresponding author

Email addresses: `Andrea.Brugnoli@isae.fr` (Andrea Brugnoli), `Daniel.Alazard@isae.fr` (Daniel Alazard), `Valerie.Budinger@isae.fr` (Valérie Pommier-Budinger), `Denis.Matignon@isae.fr` (Denis Matignon)

[1]PFEM stands for partitioned finite element method.

[2]PHs stands for port-Hamiltonian systems.

explanation of the relation between Lagrangian and Hamiltonian formulations the reader may consult [4, 5]. The main feature of this framework is its modularity. Finite-dimensional port-Hamiltonian systems can be easily interconnected together, as shown in [6], allowing the construction of complex multi-physics systems. The interconnection is possible also in the infinite-dimensional case [7], even if the procedure is not as straightforward as in the finite-dimensional case. Eventually, it is also possible to merge finite and infinite PH systems [8]. These features and capabilities are particularly appealing for control engineers in order to simplify the modeling task in preliminary analyses.

Distributed parameter systems are of relevant interest given the increased computational power available for simulations. PH distributed systems were initially presented in [9], by using the theory of differential forms. Links towards functional analysis have been made in [10] and an exhaustive reference about the subject can be found in [11]. The fundamental feature of a distributed PH system is the underlying geometric interconnection structure, the so-called Stokes-Dirac structure, that describes the power flow across the boundary and inside the system, together with an energy functional, the Hamiltonian, that determines the nature of the system. Linear/nonlinear, parabolic/hyperbolic systems can be all recast into this framework, [12]. Port-Hamiltonian systems are by definition open systems, able to interact with the environment through boundary ports. The definitions of these boundary variables is of utmost importance to show that a PH system is well posed (see [13] for the proof in the 1D case). Applications coming from continuum mechanics, electrodynamics and thermodynamics can be integrated inside this framework. Academic examples typically considered are the transmission line, the shallow water equations and the Maxwell equations [9].

Numerical simulations and control techniques require a spatial discretization that is meant to preserve the underlying properties related to power continuity. The discretization procedure for systems under PH formalism consists of two steps:

- Finite-dimensional approximation of the Stokes-Dirac structure, i.e. the formally skew symmetric differential operator that defines the structure. The duality of the power variables has to be mapped onto the finite approximation. The subspace of the discrete variables will be represented by a Dirac structure.

- The Hamiltonian requires as well a suitable discretization, which gives rise to a discrete Hamiltonian.

The research community is focusing on structure-preserving discretization techniques since several years. In [14], the authors made use of a mixed finite element spatial discretization for 1D hyperbolic system of conservation laws, introducing different low-order basis functions for the energy and co-energy variables. Pseudo-spectral methods relying on higher-order global polynomial approximations were studied in [15]. This method was used and extended to take into account unbounded control operators in [16]. More recently a simplicial discretization based on discrete exterior calculus was proposed in [17]. This approach comes with additional complexities, since a primal and a dual meshes have to be defined but the discretization is structure-preserving, regardless of the spatial dimension of the problem. Weak formulations which lead to Galerkin numerical approximations began to be explored in the last years. In [18] the prototypical example of hyperbolic systems of two conservation

law was discretized by a weak formulation. In this approach the boundary is split according to the causality of boundary ports, so that mixed boundary conditions are easily handled, but still dual meshes have to be defined.

The main contribution of this paper is the enrichment of the port-Hamiltonian formulation for the Mindlin plate model, by making use of tensor calculus [19, Chapter 16], together with a consistent discretization method. This kind of model was already presented in [20] and using the jet bundle formalism in [21] but here a novel formulation based on tensorial calculus is introduced. The second contribution of this paper concerns the extension of the Partitioned Finite Element Method (PFEM) to the Mindlin plate model. In this approach, originally presented in [22], once the system has been put into weak form, a subset of the equations is integrated by parts, so that boundary variables are naturally included into the formulation and appear as control inputs, the collocated outputs being defined accordingly. Then, the discretization of energy and co-energy variables (and the associated test functions) leads directly to a full rank representation for the finite-dimensional port-Hamiltonian system. If mixed boundary conditions are to be considered, the finite-dimensional system contains constraints, leading to an algebraic differential system (DAE), which can be treated and analyzed by referring to [23, 24]. This approach, similarly to the one detailed in [18], makes possible the usage of FEM software, like FEniCS [25]. The final discretized system can be further reduced by using appropriate model reduction techniques, as explained in [26, 27]

The paper is divided into five main sections

1. The framework of finite-dimensional port-Hamiltonian systems (PHs) and the notion of Dirac and Stokes-Dirac structures are recalled. The infinite-dimensional case is then illustrated by means of the Timoshenko beam model, the 1D counterpart of the Mindlin plate model.
2. The constitutive relations, equations of motions and energies for the Mindlin-Reissner plate are detailed.
3. The Mindlin plate port-Hamiltonian formulation is highlighted by defining energy and co-energy variables and the interconnection structure. The boundary variables are found by introducing the energy balance. Then the underlying Stokes-Dirac structure is easily obtained by defining the flow and effort spaces, together with the space of boundary variables.
4. The PFEM discretization for the Mindlin plate is detailed. The problem is put into weak form first, then the necessary integrations by parts are performed and finally the basis functions for the energy, co-energy and test functions are chosen.
5. To demonstrate the consistency of the approach an eigenvalue study of a square plate considering various boundary conditions is performed, together with some time-domain simulation.

1. Reminder on port-Hamiltonian systems

In this section the concepts of Dirac structure and Stokes-Dirac structure are recalled. From these concepts finite and infinite dimensional port-Hamiltonian system are then derived by considering the port behavior.

1.1. Dirac Structures

Consider an n-dimensional space $\mathcal{F}$ over the field $\mathbb{R}$ and $\mathcal{E} \equiv \mathcal{F}'$ its dual, i.e. the space of linear operator $\boldsymbol{e} : \mathcal{F} \to \mathbb{R}$. The elements of $\mathcal{F}$ are called flows, while the elements of $\mathcal{E}$ are called efforts. Those are port variables and their combination gives the power flowing inside the system. The space $\mathcal{B} = \mathcal{F} \times \mathcal{E}$ is called the bond space of power variables. Therefore the power is defined as $\langle \boldsymbol{e}, \boldsymbol{f} \rangle = \boldsymbol{e}(\boldsymbol{f})$, where $\langle \boldsymbol{e}, \boldsymbol{f} \rangle$ is the dual product between $\boldsymbol{f}$ and $\boldsymbol{e}$.

Definition 1 ([28], Def. 1.1.1). *Given the space $\mathcal{F}$ and its dual $\mathcal{E}$ with respect to the inner product $\langle \cdot, \cdot \rangle : \mathcal{F} \times \mathcal{E} \to \mathbb{R}$, define the symmetric bilinear form:*

$$\langle\langle (\boldsymbol{f}_1, \boldsymbol{e}_1), (\boldsymbol{f}_2, \boldsymbol{e}_2) \rangle\rangle := \langle \boldsymbol{e}_1, \boldsymbol{f}_2 \rangle + \langle \boldsymbol{e}_2, \boldsymbol{f}_1 \rangle, \quad with (\boldsymbol{f}_i, \boldsymbol{e}_i) \in \mathcal{B}, \ i = 1, 2 \tag{1}$$

A Dirac structure on $\mathcal{B} := \mathcal{F} \times \mathcal{E}$ is a subspace $\mathcal{D} \subset \mathcal{B}$, which is maximally isotropic under $\langle\langle \cdot, \cdot \rangle\rangle$.

This definition can be extended to consider distributed forces and dissipation [10].

Proposition 1. *Consider the space of power variables $\mathcal{F} \times \mathcal{E}$ and let $\mathcal{X}$ denote an n-dimensional space, the space of energy variables. Suppose that $\mathcal{F} := (\mathcal{F}_s, \mathcal{F}_e)$ and that $\mathcal{E} := (\mathcal{E}_s, \mathcal{E}_e)$, with $\dim \mathcal{F}_s = \dim \mathcal{E}_s = n$ and $\dim \mathcal{F}_e = \dim \mathcal{E}_e = m$. Moreover, let $\boldsymbol{J}(\boldsymbol{x})$ denote a skew-symmetric matrix of dimension n and by $\boldsymbol{B}(\boldsymbol{x})$ a matrix of dimension $n \times m$. Then, the set*

$$\mathcal{D} := \left\{ (\boldsymbol{f}_s, \boldsymbol{f}_e, \boldsymbol{e}_s, \boldsymbol{e}_e) \in \mathcal{F} \times \mathcal{E} \mid \quad \boldsymbol{f}_s = -\boldsymbol{J}(\boldsymbol{x})\boldsymbol{e}_s - \boldsymbol{B}(\boldsymbol{x})\boldsymbol{f}_e, \ \boldsymbol{e}_e = \boldsymbol{B}(\boldsymbol{x})^T \boldsymbol{e}_s \right\} \tag{2}$$

is a Dirac structure.

1.2. Finite-dimensional PHs

Consider the time-invariant dynamical system:

$$\begin{cases} \dot{\boldsymbol{x}} &= J(\boldsymbol{x})\nabla H(\boldsymbol{x}) + B(\boldsymbol{x})\boldsymbol{u}, \\ \boldsymbol{y} &= B(\boldsymbol{x})^T \nabla H(\boldsymbol{x}), \end{cases} \tag{3}$$

where $H(\boldsymbol{x}) : \mathcal{X} \to \mathbb{R}$, the Hamiltonian, is a real-valued function bounded from below. Such system is called port-Hamiltonian, as it arises from the Hamiltonian modelling of a physical system and it interacts with the environment through the input $\boldsymbol{u}$ included in the formulation. The connection with the concept of Dirac structure is achieved by considering the following port behavior:

$$\begin{aligned} \boldsymbol{f}_s &= -\dot{\boldsymbol{x}}, & \boldsymbol{e}_s &= \frac{\partial H}{\partial \boldsymbol{x}}, \\ \boldsymbol{f}_e &= \boldsymbol{u}, & \boldsymbol{e}_e &= \boldsymbol{y}. \end{aligned} \tag{4}$$

With this choice of the port variables system (3) defines, by proposition 1, a Dirac structure. Dissipation and distributed forces can be included and the corresponding system defines an extended Dirac structure, once the proper port variables are introduced.

1.3. Constant matrix differential operators

The treatment provided in [29] is here recovered, in order to have the most suitable definition of Stokes-Dirac structure for the mechanical systems considered in this paper. Let Ω denote a compact subset of $\mathbb{R}^d$ representing the spatial domain of the distributed parameter system. Then, let $\mathcal{U}$ and $\mathcal{V}$ denote two sets of smooth functions from Ω to $\mathbb{R}^{q_u}$ and $\mathbb{R}^{q_v}$ respectively.

Definition 2. *A constant matrix differential operator of order N is a map L from $\mathcal{U}$ to $\mathcal{V}$ such that, given $\boldsymbol{u} = (u_1, \ldots, u_{q_u}) \in \mathcal{U}$ and $\boldsymbol{v} = (v_1, ..., v_{q_v}) \in \mathcal{V}$:*

$$\boldsymbol{v} = L\boldsymbol{u} \iff \boldsymbol{v} := \sum_{|\alpha|=0}^{N} \boldsymbol{P}_\alpha D^\alpha \boldsymbol{u}, \tag{5}$$

where $\alpha := (\alpha_1, \ldots, \alpha_d)$ is a multi-index of order $|\alpha| := \sum_{i=1}^{d} \alpha_i$, $\boldsymbol{P}_\alpha$ are a set of constant real $q_v \times q_u$ matrices and $D^\alpha := \partial_{x_1}^{\alpha_1} \ldots \partial_{x_d}^{\alpha_d}$ is a differential operator of order $|\alpha|$ resulting from a combination of spatial derivatives.

Definition 3. *Consider the constant matrix differential operator (5). Its formal adjoint is the map L^* from $\mathcal{V}$ to $\mathcal{U}$ such that:*

$$\boldsymbol{u} = L^*\boldsymbol{v} \iff \boldsymbol{u} := \sum_{|\alpha|=0}^{N} (-1)^{|\alpha|} \boldsymbol{P}_\alpha^T D^\alpha \boldsymbol{v}. \tag{6}$$

Definition 4. *Let J denote a constant matrix differential operator. Then, J is skew-symmetric if and only if $J = -J^*$. This corresponds to the condition:*

$$\boldsymbol{P}_\alpha = (-1)^{|\alpha|+1} \boldsymbol{P}_\alpha^T, \quad \forall \alpha. \tag{7}$$

An important relation between a differential operator and its adjoint is expressed by the following theorem.

Theorem 1 ([30], Chapter 9, theorem 9.37)**.** *Consider a matrix differential operator L and let L^* denote its formal adjoint. Then, for each function $\boldsymbol{u} \in \mathcal{U}$ and $\boldsymbol{v} \in \mathcal{V}$:*

$$\int_\Omega \left(\boldsymbol{v}^T L\boldsymbol{u} - \boldsymbol{u}^T L^*\boldsymbol{v} \right) \, \mathrm{d}\Omega = \int_{\partial\Omega} \widetilde{B}_L(\boldsymbol{u}, \boldsymbol{v}) \, \mathrm{d}A, \tag{8}$$

where $\widetilde{B}_L$ is a differential operator induced on the boundary $\partial\Omega$ by L, or equivalently:

$$\boldsymbol{v}^T L\boldsymbol{u} - \boldsymbol{u}^T L^*\boldsymbol{v} = \operatorname{div} \widetilde{B}_L(\boldsymbol{u}, \boldsymbol{v}). \tag{9}$$

It is important to note that $\widetilde{B}_L$ is a constant differential operator. The quantity $\widetilde{B}_L(\boldsymbol{u}, \boldsymbol{v})$ is a constant linear combination of the functions $\boldsymbol{u}$ and $\boldsymbol{v}$ together with their spatial derivatives up to a certain order and depending on L.

Corollary 1. *Consider a skew-symmetric differential operator J. Then, for each function $\boldsymbol{u} \in \mathcal{U}$ and $\boldsymbol{v} \in \mathcal{V}$ with $q_u = q_v = q$:*

$$\int_\Omega \left(\boldsymbol{v}^T J\boldsymbol{u} + \boldsymbol{u}^T J\boldsymbol{v} \right) \, \mathrm{d}\Omega = \int_{\partial\Omega} \widetilde{B}_J(\boldsymbol{u}, \boldsymbol{v}) \, \mathrm{d}A, \tag{10}$$

where $\widetilde{B}_J$ is a symmetric differential operator on $\partial\Omega$ depending on the differential operator J.

1.4. Constant Stokes-Dirac structures

Following again [29] let $\mathcal{F}$ denote the space of flows, i.e. the space of smooth functions from the compact set $\Omega \subset \mathbb{R}^d$ to $\mathbb{R}^q$. For simplicity assume that the space of efforts is $\mathcal{E} \equiv \mathcal{F}$ (generally speaking these spaces are Hilbert spaces linked by duality, as in [10]). Given $\boldsymbol{f} = (f_1, \ldots, f_q) \in \mathcal{F}$ and $\boldsymbol{e} = (e_1, \ldots, e_q) \in \mathcal{E}$. Let $\boldsymbol{z} = B_\partial(\boldsymbol{e})$ denote the boundary terms, where B_∂ provides the restriction on $\partial\Omega$ of the effort e and of its spatial derivatives of proper order. Then it can be written:

$$\int_{\partial\Omega} \widetilde{B}_J(\boldsymbol{e}_1, \boldsymbol{e}_2) \, \mathrm{d}A = \int_{\partial\Omega} B_J(\boldsymbol{z}_1, \boldsymbol{z}_2) \, \mathrm{d}A, \quad \text{with} \quad \widetilde{B}_J(\cdot, \cdot) = B_J(B_\partial(\cdot), B_\partial(\cdot)). \tag{11}$$

Define the set

$$\mathcal{Z} := \{\boldsymbol{z} | \boldsymbol{z} = B_\partial(\boldsymbol{e})\}. \tag{12}$$

Theorem 2 ([29]). *Consider the space of power variables $\mathcal{B} = \mathcal{F} \times \mathcal{E} \times \mathcal{Z}$. The linear subspace $\mathcal{D} \subset \mathcal{B}$*

$$\mathcal{D} = \{(\boldsymbol{f}, \boldsymbol{e}, \boldsymbol{z}) \in \mathcal{F} \times \mathcal{E} \times \mathcal{Z} \mid \boldsymbol{f} = -J\boldsymbol{e}, \, z = B_\partial(\boldsymbol{e})\}, \tag{13}$$

is a Stokes–Dirac structure on $\mathcal{B}$ with respect to the pairing

$$\langle\langle(\boldsymbol{f}_1, \boldsymbol{e}_1, \boldsymbol{z}_1), (\boldsymbol{f}_2, \boldsymbol{e}_2, \boldsymbol{z}_2)\rangle\rangle := \int_\Omega \left(\boldsymbol{e}_1^T \boldsymbol{f}_2 + \boldsymbol{e}_2^T \boldsymbol{f}_1\right) \, \mathrm{d}\Omega + \int_{\partial\Omega} B_J(\boldsymbol{z}_1, \boldsymbol{z}_2) \, \mathrm{d}A. \tag{14}$$

Remark 1. *The constant Stokes-Dirac structure has been defined in case of smooth vector valued functions for simplicity. In this context the pairing has been defined as the L^2 inner product of vector-valued function. The definition is indeed more general and encompasses the case of more complex functional spaces. The Mindlin plate for example is defined on a mixed function space of scalar-, vector- and tensor- valued functions. The result presented here remains valid provided that the proper pairing is being chosen. Furthermore, the constant differential operator may contain intrinsic operators (div, grad) as it will be shown for the Mindlin plate case.*

1.5. Infinite-dimensional PHs

Following [11, Chapter 3], the prototypical example of the Timoshenko beam will be used to illustrate the class of distributed port-Hamiltonian systems. This model consists of two coupled PDEs, describing the vertical displacement and rotation scalar fields:

$$\begin{cases} \rho(x)\dfrac{\partial^2 w}{\partial t^2}(x,t) & = \dfrac{\partial}{\partial x}\left[K(x)\left(\dfrac{\partial w}{\partial x}(x,t) - \phi(x,t)\right)\right], \quad x \in (0, L), \, t \geq 0 \\ I_\rho(x)\dfrac{\partial^2 \phi}{\partial t^2}(x,t) & = \dfrac{\partial}{\partial x}\left(EI(x)\dfrac{\partial \phi}{\partial x}(x,t)\right) + K(x)\left(\dfrac{\partial w}{\partial x}(x,t) - \phi(x,t)\right), \end{cases} \tag{15}$$

where $w(x,t)$ is the transverse displacement and $\phi(x,t)$ is the rotation angle of a fiber of the beam. The coefficients $\rho(x), I_\rho(x), E(x), I(x)$ and $K(x)$ are the mass per unit length, the rotary moment of inertia of a cross section, Young's modulus of elasticity, the moment of inertia of a cross section and the shear modulus, respectively. The energy variables are

chosen as follows:

$$
\begin{aligned}
\alpha_w &:= \rho(x)\frac{\partial w}{\partial t}(x,t), && \text{Linear Momentum,} \\
\alpha_\phi &:= I_\rho(x)\frac{\partial \phi}{\partial t}(x,t), && \text{Angular Momentum,} \\
\alpha_\kappa &:= \frac{\partial \phi}{\partial x}(x,t), && \text{Curvature,} \\
\alpha_\gamma &:= \frac{\partial w}{\partial x}(x,t) - \phi(x,t), && \text{Shear Deformation.}
\end{aligned}
\tag{16}
$$

Those variables are collected in the vector $\boldsymbol{\alpha} := (\alpha_w,\ \alpha_\phi,\ \alpha_\kappa,\ \alpha_\gamma)^T$, so that the Hamiltonian can be written as a quadratic functional in the energy variables:

$$
H = \frac{1}{2}\int_0^L \boldsymbol{\alpha}^T Q \boldsymbol{\alpha}\, dx, \qquad \text{where} \qquad Q = \begin{bmatrix} \frac{1}{\rho(x)} & 0 & 0 & 0 \\ 0 & \frac{1}{I_\rho(x)} & 0 & 0 \\ 0 & 0 & EI(x) & 0 \\ 0 & 0 & 0 & K(x) \end{bmatrix}.
\tag{17}
$$

The co-energy variables are found by computing the variational derivative of the Hamiltonian (see [31]):

$$
\begin{aligned}
e_w &:= \frac{\delta H}{\delta \alpha_w} = \frac{\partial w}{\partial t}(x,t), && \text{Linear Velocity,} \\
e_\phi &:= \frac{\delta H}{\delta \alpha_\phi} = \frac{\partial \phi}{\partial t}(x,t), && \text{Angular Velocity,} \\
e_\kappa &:= \frac{\delta H}{\delta \alpha_\kappa} = EI(x)\frac{\partial \phi}{\partial x}(x,t), && \text{Flexural Momentum,} \\
e_\gamma &:= \frac{\delta H}{\delta \alpha_\gamma} = K(x)\left(\frac{\partial w}{\partial x}(x,t) - \phi(x,t)\right), && \text{Shear Force.}
\end{aligned}
\tag{18}
$$

These variables are again collected in the vector $\boldsymbol{e} = (e_w,\ e_\phi,\ e_\kappa,\ e_\gamma)^T$, so that system (15) can be rewritten in terms of energy and co-energy variables:

$$
\frac{\partial \boldsymbol{\alpha}}{\partial t} = J\mathbf{e}, \qquad \text{where} \qquad J = \begin{bmatrix} 0 & 0 & 0 & \frac{\partial}{\partial x} \\ 0 & 0 & \frac{\partial}{\partial x} & 1 \\ 0 & \frac{\partial}{\partial x} & 0 & 0 \\ \frac{\partial}{\partial x} & -1 & 0 & 0 \end{bmatrix}.
\tag{19}
$$

By Definition (4), the constant matrix differential operator J is skew-symmetric. In order to unveil the Stokes-Dirac structure for this model, boundary variables have to be defined. The energy rate is given by (see [11] for a detailed derivation):

$$
\dot{H} = \boldsymbol{f}_\partial^T \boldsymbol{e}_\partial,
\tag{20}
$$

where

$$
\begin{aligned}
\boldsymbol{f}_\partial &= \begin{bmatrix} e_w(0) & e_\phi(0) & e_\gamma(L) & e_\kappa(L) \end{bmatrix}^T, \\
\boldsymbol{e}_\partial &= \begin{bmatrix} -e_\gamma(0) & -e_\kappa(0) & e_w(L) & e_\phi(L) \end{bmatrix}^T.
\end{aligned}
\tag{21}
$$

7

Consider now the power space

$$\mathcal{B} := \{(\boldsymbol{f}, \boldsymbol{e}, \boldsymbol{z}) \in \mathcal{F} \times \mathcal{E} \times \mathcal{Z}\}, \tag{22}$$

where $\mathcal{F} \equiv \mathcal{E} = L^2((0, L); \mathbb{R}^4)$ and

$$\mathcal{Z} := \left\{\boldsymbol{z} \mid \boldsymbol{z} = \begin{pmatrix} \boldsymbol{f}_\partial \\ \boldsymbol{e}_\partial \end{pmatrix}\right\}. \tag{23}$$

The duality pairing between elements of $\mathcal{B}$ is then defined as follows:

$$\langle\langle(\boldsymbol{f}_1, \boldsymbol{e}_1, \boldsymbol{z}_1), (\boldsymbol{f}_2, \boldsymbol{e}_2, \boldsymbol{z}_2)\rangle\rangle := \int_0^L \left(\boldsymbol{e}_1^T \boldsymbol{f}_2 + \boldsymbol{e}_2^T \boldsymbol{f}_1\right) \, \mathrm{d}x + B_J(\boldsymbol{z}_1, \boldsymbol{z}_2), \tag{24}$$

where $B_J(\boldsymbol{z}_1, \boldsymbol{z}_2) := (\boldsymbol{f}_{\partial,1})^T \boldsymbol{e}_{\partial,2} + (\boldsymbol{f}_{\partial,2})^T \boldsymbol{e}_{\partial,1}$. It is now possible to state the following theorem:

Theorem 3 (Stokes-Dirac Structure for the Timoshenko beam). *Consider the space of power variables $\mathcal{B}$ defined in (22). By theorem 2 the linear subspace $\mathcal{D} \subset \mathcal{B}$*

$$\mathcal{D} = \left\{(\boldsymbol{f}, \boldsymbol{e}, \boldsymbol{z}) \in \mathcal{B} \mid \boldsymbol{f} = -\frac{\partial \boldsymbol{\alpha}}{\partial t} = -J\boldsymbol{e}, \ \boldsymbol{z} = \begin{pmatrix} \boldsymbol{f}_\partial \\ \boldsymbol{e}_\partial \end{pmatrix}\right\}, \tag{25}$$

is a Stokes-Dirac structure with respect to the pairing $\langle\langle\cdot, \cdot\rangle\rangle$ given by (24).

2. Mindlin theory for thick plates

In this section the classical model of thick plates is first recalled by making use of a tensorial formalism to simplify the discussion on the port-Hamiltonian formulation. The Mindlin plate theory, originally presented in [32], is more suited for plates having a large thickness. The fibers, i.e. a segment perpendicular to the mid-plane, of the plate are supposed to remain straight after the deformation, but not necessarily normal to the mid-plane. For this reason two new kinematic variables have to be added, in order to represent the deflection of the cross sections. Let θ_x denote the deflection of the cross section with respect to the opposite side of the y axis and θ_y its deflection along the x axis. The displacement field is therefore given by the following relations:

$$\begin{aligned} u(x, y, z) &= -z\theta_x(x, y), & \text{Displacement along } x, \\ v(x, y, z) &= -z\theta_y(x, y), & \text{Displacement along } y, \\ w(x, y, z) &= w(x, y), & \text{Displacement along } z. \end{aligned} \tag{26}$$

Both bending and shear deformations are taken into account. The bending part is described by the second order shear tensor:

$$\mathbb{E}_b = \begin{bmatrix} \epsilon_{xx} & \gamma_{xy} \\ \gamma_{xy} & \epsilon_{yy} \end{bmatrix} = -z \, \mathrm{Grad}(\boldsymbol{\theta}) = -z \begin{bmatrix} \frac{\partial \theta_x}{\partial x} & \frac{1}{2}\left(\frac{\partial \theta_y}{\partial x} + \frac{\partial \theta_x}{\partial y}\right) \\ \frac{1}{2}\left(\frac{\partial \theta_y}{\partial x} + \frac{\partial \theta_x}{\partial y}\right) & \frac{\partial \theta_y}{\partial y} \end{bmatrix}, \tag{27}$$

where $\boldsymbol{\theta} = (\theta_x, \theta_y)^T$. The tensor $\mathrm{Grad}(\boldsymbol{\theta})$ stands for the symmetric gradient of the vector $\boldsymbol{\theta}$ and corresponds to the curvature tensor:

$$\mathbb{K} = \begin{bmatrix} \kappa_{xx} & \kappa_{xy} \\ \kappa_{xy} & \kappa_{yy} \end{bmatrix} := \mathrm{Grad}(\boldsymbol{\theta}) = \frac{1}{2}\left(\nabla \otimes \boldsymbol{\theta} + (\nabla \otimes \boldsymbol{\theta})^T\right), \tag{28}$$

where $\boldsymbol{u} \otimes \boldsymbol{v}$ denotes the outer product of vectors, equivalent to the dyadic product given by $\boldsymbol{u}\boldsymbol{v}^T$. The corresponding bending stress field $\mathbb{S}_b$ is obtained by considering the constitutive relation which, for an isotropic homogeneous material, reads:

$$\mathbb{S}_b = \frac{E}{1-\nu^2} \left\{ (1-\nu)\mathbb{E}_b + \nu \boldsymbol{I}_{2\times 2} \operatorname{Tr}(\mathbb{E}_b) \right\}, \tag{29}$$

where E is Young's modulus, ν Poisson's ratio, $\boldsymbol{I}_{2\times 2}$ the identity operator in $\mathbb{R}^2$ and Tr the trace operator. By averaging the torques produced by stresses along a fiber, it is possible to define the flexural momenta tensor:

$$\mathbb{M}_{ij} = \int_{-\frac{h}{2}}^{\frac{h}{2}} -z \, \mathbb{S}_{b,\,ij} \, \mathrm{d}z = \mathbb{D}_{ijkl} \, \mathbb{K}_{kl}, \tag{30}$$

where h is the plate thickness and $\mathbb{D}$ is the a fourth order symmetric tensor and represents the bending rigidity tensor. The components of the momenta tensor are given by the following relations:

$$\mathbb{M} = \begin{bmatrix} M_{xx} & M_{xy} \\ M_{xy} & M_{yy} \end{bmatrix}, \qquad \begin{aligned} M_{xx} &= D\left(\kappa_{xx} + \nu\kappa_{yy}\right), \\ M_{yy} &= D\left(\kappa_{yy} + \nu\kappa_{xx}\right), \\ M_{xy} &= D\left(1-\nu\right)\kappa_{xy}, \end{aligned} \tag{31}$$

where $D = \frac{Eh^3}{12(1-\nu^2)}$ is the bending rigidity. The shear deformations are described using the shear strain vector:

$$\boldsymbol{\epsilon}_s = \begin{pmatrix} \gamma_{xz} \\ \gamma_{yz} \end{pmatrix} = \begin{pmatrix} \frac{\partial w}{\partial x} - \theta_x \\ \frac{\partial w}{\partial y} - \theta_y \end{pmatrix}. \tag{32}$$

The corresponding stress field is simply given by $\boldsymbol{\sigma}_s = G\boldsymbol{\epsilon}_s$, where G is the shear modulus $G = \frac{E}{2(1+\nu)}$. The shear forces are again obtained by averaging the shear stress along plate fibers. However, given the excessive rigidity of the shear contribution, a correction factor $k = 5/6$ (see [32]) is introduced:

$$\boldsymbol{q} = \begin{pmatrix} q_x \\ q_y \end{pmatrix} = \int_{-\frac{h}{2}}^{\frac{h}{2}} k\boldsymbol{\sigma}_s \, \mathrm{d}z = kGh \, \boldsymbol{\epsilon}_s = kGh \begin{pmatrix} \gamma_{xz} \\ \gamma_{yz} \end{pmatrix}. \tag{33}$$

All the needed variables are now defined and the equations of motions can be recalled (see [32]):

$$\begin{cases} \rho h \dfrac{\partial^2 w}{\partial t^2} &= \operatorname{div}(\boldsymbol{q}), \\ \rho \dfrac{h^3}{12} \dfrac{\partial^2 \boldsymbol{\theta}}{\partial t^2} &= \boldsymbol{q} + \operatorname{Div}(\mathbb{M}), \end{cases} \tag{34}$$

where ρ is the plate mass density. The differential operators div() and Div() denote the divergence of a vector and of a tensor, respectively:

$$\boldsymbol{a} = \operatorname{Div}(\mathbb{A}) \qquad \text{with } \boldsymbol{a}_i = \operatorname{div}(\mathbb{A}_{ji}) = \sum_{j=1}^{n} \frac{\partial \mathbb{A}_{ji}}{\partial x_j},$$

where $\boldsymbol{a}$ is defined column-wise. The kinetic and potential energy densities per unit area ($\mathcal{K}$ and $\mathcal{U}$), are given respectively by:

$$\mathcal{K} = \frac{1}{2}\rho \left\{ h \left(\frac{\partial w}{\partial t} \right)^2 + \frac{h^3}{12} \frac{\partial \boldsymbol{\theta}}{\partial t} \cdot \frac{\partial \boldsymbol{\theta}}{\partial t} \right\},$$

$$\mathcal{U} = \frac{1}{2} \left\{ \mathbb{M} : \mathbb{K} + \boldsymbol{q} \cdot \boldsymbol{\epsilon}_s \right\}.$$

where the tensor contraction $\mathbb{M} : \mathbb{K}$ in Cartesian coordinates is expressed as:

$$\mathbb{M} : \mathbb{K} = \sum_{i,j=1}^{2} M_{ij}\kappa_{ij} = \mathrm{Tr}(\mathbb{M}^T \mathbb{K}).$$

The total energy density is the sum of kinetic and potential energies

$$\mathcal{H} = \mathcal{K} + \mathcal{U} \tag{35}$$

and the corresponding energies

$$H = \int_\Omega \mathcal{H} \ \mathrm{d}\Omega, \qquad K = \int_\Omega \mathcal{K} \ \mathrm{d}\Omega, \qquad U = \int_\Omega \mathcal{U} \ \mathrm{d}\Omega, \tag{36}$$

where Ω is an open connected set of $\mathbb{R}^2$.

3. PH tensorial formulation of the Mindlin plate

In this section the new tensorial formulation for the Mindlin plate is presented. Obviously this result is equivalent to the one found in the vectorial case [20], but the tensorial formulation is more suitable from the point of view of functional analysis since it makes appear intrinsic operators (div, Div, grad, Grad) as it will be shown in the following, regardless of the choice of coordinate frame.

The Hamiltonian energy is first considered in order to find the proper energy variables:

$$H = \int_\Omega \frac{1}{2} \left\{ \rho h \left(\frac{\partial w}{\partial t} \right)^2 + \frac{\rho h^3}{12} \frac{\partial \boldsymbol{\theta}}{\partial t} \cdot \frac{\partial \boldsymbol{\theta}}{\partial t} + \mathbb{M} : \mathbb{K} + \boldsymbol{q} \cdot \boldsymbol{\epsilon}_s \right\} \mathrm{d}\Omega, \tag{37}$$

The choice of the energy variables is the same as in [20] but here scalar, vector and tensor variables are gathered together:

$$
\begin{array}{llll}
\alpha_w = \rho h \dfrac{\partial w}{\partial t}, & \text{Linear momentum,} & \boldsymbol{\alpha}_\theta = \dfrac{\rho h^3}{12} \dfrac{\partial \boldsymbol{\theta}}{\partial t}, & \text{Angular momentum,} \\
\mathbb{A}_\kappa = \mathbb{K}, & \text{Curvature Tensor,} & \boldsymbol{\alpha}_\gamma = \boldsymbol{\epsilon}_s. & \text{Shear Deformation.}
\end{array}
\tag{38}
$$

The co-energy variables are found by computing the variational derivative of the Hamiltonian:

$$
\begin{array}{llll}
e_w := \dfrac{\delta H}{\delta \alpha_w} = \dfrac{\partial w}{\partial t}, & \text{Linear velocity,} & \boldsymbol{e}_\theta := \dfrac{\delta H}{\delta \boldsymbol{\alpha}_\theta} = \dfrac{\partial \boldsymbol{\theta}}{\partial t}, & \text{Angular momentum,} \\
\mathbb{E}_\kappa := \dfrac{\delta H}{\delta \mathbb{A}_\kappa} = \mathbb{M}, & \text{Momenta Tensor,} & \boldsymbol{e}_\gamma := \dfrac{\delta H}{\delta \boldsymbol{\epsilon}_s} = \boldsymbol{q} & \text{Shear stress.}
\end{array}
\tag{39}
$$

Proposition 2. *The variational derivative of the Hamiltonian with respect to the curvature tensor is the momenta tensor* $\frac{\delta H}{\delta \mathbb{A}_\kappa} = \mathbb{M}$.

Proof. The contribution due to the bending part in Hamiltonian is given by:

$$H_b(\mathbb{K}) = \frac{1}{2} \int_\Omega \mathbb{M} : \mathbb{K} \ \mathrm{d}\Omega = \frac{1}{2} \int_\Omega \mathrm{Tr}(\mathbb{M}^T \mathbb{K}) \ \mathrm{d}\Omega,$$

where the momenta tensor depends on the curvatures tensor $\mathbb{M}_{ij} = \mathbb{D}_{ijkl}\mathbb{K}_{kl}$ where $\mathbb{D} = \mathbb{D}^T$ is a fourth order symmetric positive definite tensor. So a variation $\delta\mathbb{K}$ of the curvatures tensor with respect to a given value $\mathbb{K}_0$ leads to:

$$H_b(\mathbb{K}_0 + \varepsilon\delta\mathbb{K}) = \frac{1}{2} \int_\Omega \mathrm{Tr}(\mathbb{M}_0^T \mathbb{K}_0) \ \mathrm{d}\Omega + \varepsilon\frac{1}{2} \int_\Omega \left\{ \mathrm{Tr}(\mathbb{M}_0^T\delta\mathbb{K}) + \mathrm{Tr}(\delta\mathbb{M}^T\mathbb{K}_0) \right\} \ \mathrm{d}\Omega + O(\varepsilon^2).$$

The term $\mathrm{Tr}(\delta\mathbb{M}^T\mathbb{K}_0)$ can be further manipulated as follows

$$\mathrm{Tr}(\delta\mathbb{M}^T\mathbb{K}_0) = \mathrm{Tr}(\mathbb{K}_0^T\delta\mathbb{M}) = \mathrm{Tr}(\mathbb{K}_0^T \mathbb{D} \,\delta\mathbb{K}) = \mathrm{Tr}(\mathbb{M}_0^T\delta\mathbb{K}),$$

so that

$$H_b(\mathbb{K}_0 + \varepsilon\delta\mathbb{K}) = \frac{1}{2} \int_\Omega \mathrm{Tr}(\mathbb{M}_0^T \mathbb{K}_0) \ \mathrm{d}\Omega + \varepsilon \int_\Omega \left\{ \mathrm{Tr}(\mathbb{M}_0^T\delta\mathbb{K}) \right\} \ \mathrm{d}\Omega + O(\varepsilon^2).$$

By definition of the variational derivative (see e.g. [9]) it can be written:

$$H_b(\mathbb{K}_0 + \varepsilon\delta\mathbb{K}) = H_b(\mathbb{K}_0) + \varepsilon \left\langle \frac{\delta H_b}{\delta\mathbb{K}}, \delta\mathbb{K} \right\rangle_{\mathscr{H}} + O(\varepsilon^2),$$

where $\mathscr{H}$ is the space of the square integrable symmetric tensors endowed with the integral of the tensor contraction as inner product. Then, by identification $\frac{\delta H_b}{\delta\mathbb{K}} = \frac{\delta H}{\delta\mathbb{K}} = \mathbb{M}_0$. $\square$

The port-Hamiltonian system is expressed as follows:

$$\begin{cases} \dfrac{\partial \alpha_w}{\partial t} &= \mathrm{div}(\boldsymbol{e}_\gamma), \\[2mm] \dfrac{\partial \boldsymbol{\alpha}_\theta}{\partial t} &= \mathrm{Div}(\mathbb{E}_\kappa) + \boldsymbol{e}_\gamma, \\[2mm] \dfrac{\partial \mathbb{A}_\kappa}{\partial t} &= \mathrm{Grad}(\boldsymbol{e}_\theta), \\[2mm] \dfrac{\partial \boldsymbol{\alpha}_\gamma}{\partial t} &= \mathrm{grad}(e_w) - \boldsymbol{e}_\theta, \end{cases} \tag{40}$$

If the variables are concatenated together, the formally skew-symmetric operator J can be highlighted:

$$\frac{\partial}{\partial t} \begin{pmatrix} \alpha_w \\ \boldsymbol{\alpha}_\theta \\ \mathbb{A}_\kappa \\ \boldsymbol{\alpha}_\gamma \end{pmatrix} = \underbrace{\begin{bmatrix} 0 & 0 & 0 & \mathrm{div} \\ 0 & 0 & \mathrm{Div} & \boldsymbol{I}_{2\times2} \\ 0 & \mathrm{Grad} & 0 & 0 \\ \mathrm{grad} & -\boldsymbol{I}_{2\times2} & 0 & 0 \end{bmatrix}}_{J} \begin{pmatrix} e_w \\ \boldsymbol{e}_\theta \\ \mathbb{E}_\kappa \\ \boldsymbol{e}_\gamma \end{pmatrix}, \tag{41}$$

where all zeros are intended as nullifying operators from the space of input variables to the space of output variables.

Remark 2. *It can be observed that the interconnection structure given by J in* (41) *mimics that of the Timoshenko beam given in* (19).

Theorem 4. *The adjoint of the tensor divergence* Div *is* $-$Grad, *the opposite of the symmetric gradient.*

Proof. Let us consider the Hilbert space of the square integrable symmetric tensors of size $n \times n$ over an open connected set Ω. This space will be denoted by $\mathscr{H}_1 = L^2(\Omega, \mathbb{R}^{n \times n}_{\mathrm{sym}})$. This space is endowed with the integral of the tensor contraction as scalar product:

$$\langle \mathbb{E}, \mathbb{F} \rangle_{\mathscr{H}_1} = \int_\Omega \mathbb{E} : \mathbb{F} \ \mathrm{d}\Omega = \int_\Omega \mathrm{Tr}(\mathbb{E}^T \mathbb{F}) \ \mathrm{d}\Omega, \quad \forall \mathbb{E}, \mathbb{F} \in L^2(\Omega, \mathbb{R}^{n \times n}_{\mathrm{sym}}).$$

Moreover the Hilbert space of the square integrable vector functions over the same open connected set Ω will be denoted by $\mathscr{H}_2 = L^2(\Omega, \mathbb{R}^n)$. This space is endowed with the following scalar product:

$$\langle \boldsymbol{\varepsilon}, \boldsymbol{\phi} \rangle_{\mathscr{H}_2} = \int_\Omega \boldsymbol{\varepsilon} \cdot \boldsymbol{\phi} \ \mathrm{d}\Omega = \int_\Omega \boldsymbol{\varepsilon}^T \boldsymbol{\phi} \ \mathrm{d}\Omega, \quad \forall \boldsymbol{\varepsilon}, \boldsymbol{\phi} \in L^2(\Omega, \mathbb{R}^n).$$

Let us consider the tensor divergence operator defined as:

$$A : \ \mathscr{H}_1 \to \mathscr{H}_2, \qquad \text{with } \boldsymbol{\varepsilon}_i = \mathrm{div}(\mathbb{E}_{ji}) = \sum_{j=1}^n \frac{\partial \mathbb{E}_{ji}}{\partial x_j}.$$
$$\mathbb{E} \to \mathrm{Div}(\mathbb{E}) = \boldsymbol{\varepsilon},$$

We try to identify A^*

$$A^* : \ \mathscr{H}_2 \to \mathscr{H}_1,$$
$$\boldsymbol{\phi} \to A^* \boldsymbol{\phi} = \mathbb{F},$$

such that

$$\langle A\mathbb{E}, \boldsymbol{\phi} \rangle_{\mathscr{H}_2} = \langle \mathbb{E}, A^* \boldsymbol{\phi} \rangle_{\mathscr{H}_1}, \qquad \begin{matrix} \forall \mathbb{E} \in \mathrm{Domain}(A) \subset \mathscr{H}_1 \\ \forall \boldsymbol{\phi} \in \mathrm{Domain}(A^*) \subset \mathscr{H}_2 \end{matrix}$$

Now let us take $\mathbb{E} \in \mathcal{C}_0^1(\Omega, \mathbb{R}^{n \times n}_{\mathrm{sym}}) \subset \mathrm{Domain}(A)$ the space of differentiable symmetric tensors with compact support in Ω. Additionally $\boldsymbol{\phi}$ will belong to $\mathcal{C}_0^1(\Omega, \mathbb{R}^n) \subset \mathrm{Domain}(A^*)$, the space of differentiable vector functions with compact support in Ω. Then

$$\langle \mathrm{Div}\mathbb{E}, \boldsymbol{\phi} \rangle_{\mathscr{H}_2} = \int_\Omega \boldsymbol{\varepsilon} \cdot \boldsymbol{\phi} \ \mathrm{d}\Omega$$
$$= \int_\Omega \sum_{i=1}^n \sum_{j=1}^n \frac{\partial \mathbb{E}_{ji}}{\partial x_j} \phi_i \ \mathrm{d}\Omega,$$
$$= -\int_\Omega \sum_{i=1}^n \sum_{j=1}^n \mathbb{E}_{ji} \frac{\partial \phi_i}{\partial x_j} \ \mathrm{d}\Omega, \qquad \text{since the functions vanish at the boundary,}$$
$$= -\int_\Omega \sum_{i=1}^n \sum_{j=1}^n \mathbb{E}_{ji} \mathbb{F}_{ji} \ \mathrm{d}\Omega, \qquad \text{if we first choose} \quad \mathbb{F}_{ji} = \frac{\partial \phi_i}{\partial x_j}.$$

But in this latter case, it could not indeed be stated that $\mathbb{F} \in L^2(\Omega, \mathbb{R}^{n \times n}_{\mathrm{sym}})$. Now, since $\mathbb{E} \in L^2(\Omega, \mathbb{R}^{n \times n}_{\mathrm{sym}})$, $\mathbb{E}_{ji} = \mathbb{E}_{ij}$, thus we are allowed to further decompose the last equality as:
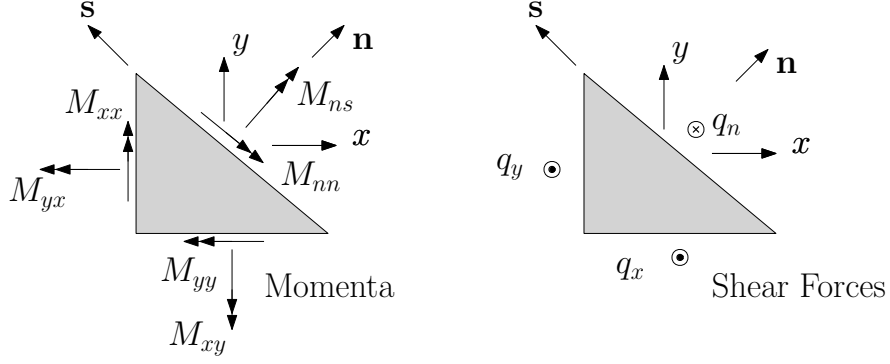
12

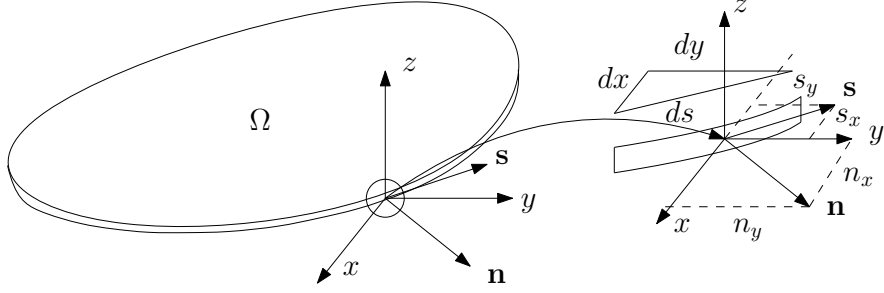Figure 1: Cauchy law for momenta and forces at the boundary.

Figure 2: Reference frames and notations.

$$\sum_{i,j} \mathbb{E}_{ji}\frac{\partial \phi_i}{\partial x_j} = \sum_{i,j} \mathbb{E}_{ji}\frac{1}{2}\left(\frac{\partial \phi_i}{\partial x_j} + \frac{\partial \phi_j}{\partial x_i}\right) = \sum_{i,j} \mathbb{E}_{ji}\mathbb{F}_{ji}, \qquad \text{with } \mathbb{F}_{ji} := \frac{1}{2}\left(\frac{\partial \phi_i}{\partial x_j} + \frac{\partial \phi_j}{\partial x_i}\right).$$

Thus $\mathbb{F} \in L^2(\Omega, \mathbb{R}^{n\times n}_{\text{sym}})$ and it can be stated that:

$$\langle \text{Div}\mathbb{E}, \boldsymbol{\phi}\rangle_{\mathcal{H}_2} = -\int_\Omega \sum_{i,j} \mathbb{E}_{ji}\frac{1}{2}\left(\frac{\partial \phi_i}{\partial x_j} + \frac{\partial \phi_j}{\partial x_i}\right) \ \mathrm{d}\Omega = -\int_\Omega \sum_{i,j} \mathbb{E}_{ji}\mathbb{F}_{ji} \ \mathrm{d}\Omega = \langle \mathbb{E}, -\text{Grad}\boldsymbol{\phi}\rangle_{\mathcal{H}_1}.$$

It can be concluded that the formal adjoint of Div is $\text{Div}^* = -\text{Grad}$. $\qquad\square$

We shall now establish the total energy balance in terms of boundary variables. Those will then be part of the underlying Stokes-Dirac structure of this model:

$$\begin{aligned}
\dot{H} &= \int_\Omega \left\{\frac{\partial \alpha_w}{\partial t}e_w + \frac{\partial \boldsymbol{\alpha}_\theta}{\partial t}\cdot\boldsymbol{e}_\theta + \frac{\partial \mathbb{A}_\kappa}{\partial t}:\mathbb{E}_\kappa + \frac{\partial \boldsymbol{\alpha}_\gamma}{\partial t}\cdot\boldsymbol{e}_\gamma\right\} \ \mathrm{d}\Omega \\
&= \int_\Omega \left\{\text{div}(\boldsymbol{e}_\gamma)e_w + \text{Div}(\mathbb{E}_\kappa)\cdot\boldsymbol{e}_\theta + \ \text{Grad}(\boldsymbol{e}_\theta):\mathbb{E}_\kappa + \text{grad}(e_w)\cdot\boldsymbol{e}_\gamma\right\} \ \mathrm{d}\Omega \qquad (42) \\
&= \int_{\partial\Omega} \left\{w_t\, q_n + \omega_n\, M_{nn} + \omega_s\, M_{ns}\right\} \ \mathrm{d}s,
\end{aligned}$$

where s is the curvilinear abscissa. The last integral is obtained by applying Green-Gauss theorem. The boundary variables appearing in the last line of (42) and illustrated in Figure

13

are defined as follows:

$$\begin{aligned}
\text{Shear Force} \quad & q_n := \boldsymbol{q} \cdot \boldsymbol{n} = \boldsymbol{e}_\gamma \cdot \boldsymbol{n}, \\
\text{Flexural momentum} \quad & M_{nn} := \mathbb{M} : (\boldsymbol{n} \otimes \boldsymbol{n}) = \mathbb{E}_\kappa : (\boldsymbol{n} \otimes \boldsymbol{n}), \\
\text{Torsional momentum} \quad & M_{ns} := \mathbb{M} : (\boldsymbol{s} \otimes \boldsymbol{n}) = \mathbb{E}_\kappa : (\boldsymbol{s} \otimes \boldsymbol{n}),
\end{aligned} \tag{43}$$

Vectors $\boldsymbol{n}$ and $\boldsymbol{s}$ designate the normal and tangential unit vectors to the boundary, as shown in Figure 2. The corresponding power conjugated variables are:

$$\begin{aligned}
\text{Vertical velocity} \quad & w_t := \frac{\partial w}{\partial t} = e_w, \\
\text{Flexural rotation} \quad & \omega_n := \frac{\partial \boldsymbol{\theta}}{\partial t} \cdot \boldsymbol{n} = \boldsymbol{e}_\theta \cdot \boldsymbol{n}, \\
\text{Torsional rotation} \quad & \omega_s := \frac{\partial \boldsymbol{\theta}}{\partial t} \cdot \boldsymbol{s} = \boldsymbol{e}_\theta \cdot \boldsymbol{s}.
\end{aligned} \tag{44}$$

Analogously to the Timoshenko beam case, the Stokes-Dirac structure for the Mindlin plate can now be defined. Consider now the bond space:

$$\mathcal{B} := \{ (\boldsymbol{f}, \boldsymbol{e}, \boldsymbol{z}) \in \mathcal{F} \times \mathcal{E} \times \mathcal{Z} \}, \tag{45}$$

where $\mathcal{F} = \mathscr{L}^2(\Omega) := L^2(\Omega) \times L^2(\Omega; \mathbb{R}^2) \times L^2(\Omega, \mathbb{R}^{2\times2}_{\text{sym}}) \times L^2(\Omega; \mathbb{R}^2)$ and $\mathcal{E} = \mathscr{H}^1(\Omega) = H^1(\Omega) \times H^1(\Omega, \mathbb{R}^2) \times H^{\text{Div}}(\Omega, \mathbb{R}^{2\times2}_{\text{sym}}) \times H^{\text{div}}(\Omega, \mathbb{R}^2)$. Consider the space of boundary port variables:

$$\mathcal{Z} := \left\{ \boldsymbol{z} \mid \boldsymbol{z} = \begin{pmatrix} \boldsymbol{f}_\partial \\ \boldsymbol{e}_\partial \end{pmatrix} \right\}, \quad \text{with} \quad \boldsymbol{f}_\partial = \begin{pmatrix} w_t \\ \omega_n \\ \omega_s \end{pmatrix} \quad \text{and} \quad \boldsymbol{e}_\partial = \begin{pmatrix} q_n \\ M_{nn} \\ M_{ns} \end{pmatrix} \tag{46}$$

The duality pairing between elements of $\mathcal{B}$ is then defined as follows:

$$\langle\langle (\boldsymbol{f}_1, \boldsymbol{e}_1, \boldsymbol{z}_1), (\boldsymbol{f}_2, \boldsymbol{e}_2, \boldsymbol{z}_2) \rangle\rangle := \langle \boldsymbol{e}_1, \boldsymbol{f}_2 \rangle_{\mathscr{L}^2(\Omega)} + \langle \boldsymbol{e}_2, \boldsymbol{f}_1 \rangle_{\mathscr{L}^2(\Omega)} + \int_{\partial\Omega} B_J(\boldsymbol{z}_1, \boldsymbol{z}_2) \, \mathrm{d}s, \tag{47}$$

where the pairing $\langle \cdot, \cdot \rangle_{\mathscr{L}^2(\Omega)}$ is the L^2 inner product on space $\mathscr{L}^2(\Omega)$ and $B_J(\boldsymbol{z}_1, \boldsymbol{z}_2) := (\boldsymbol{f}_{\partial,1})^T \boldsymbol{e}_{\partial,2} + (\boldsymbol{f}_{\partial,2})^T \boldsymbol{e}_{\partial,1}$.

Theorem 5 (Stokes-Dirac Structure for the Mindlin plate in tensorial form)**.** *Consider the space of power variables $\mathcal{B}$ defined in (45) and the matrix differential operator J in (41). By theorem 2, the linear subspace $\mathcal{D} \subset \mathcal{B}$:*

$$\mathcal{D} = \left\{ (\boldsymbol{f}, \boldsymbol{e}, \boldsymbol{z}) \in \mathcal{B} \mid \boldsymbol{f} = -\frac{\partial \boldsymbol{\alpha}}{\partial t} = -J\boldsymbol{e}, \ \boldsymbol{z} = \begin{pmatrix} \boldsymbol{f}_\partial \\ \boldsymbol{e}_\partial \end{pmatrix} \right\}, \tag{48}$$

is a Stokes-Dirac structure with respect to the pairing $\langle\langle \cdot, \cdot \rangle\rangle$ given by (47).

Remark 3. *The Hamiltonian formulation and associated Stokes-Dirac structure involve a Hamiltonian skew-symmetric differential operator J on the space $\mathcal{E}$ of the coenergy variables. This represents a significant difference with respect to the Hamiltonian system obtained by the Legendre transformation of the Euler-Lagrange system [21]. In the former formulation*

the total dimension of this system is 8, in the latter 6. Furthermore, the latter system is ruled by an algebraic operator, the differential part being hidden in the variational derivative of the Hamiltonian, leading to the following system:

$$
\begin{pmatrix} w \\ \theta_x \\ \theta_y \\ p_w \\ p_{\theta,x} \\ p_{\theta,y} \end{pmatrix} = \begin{bmatrix} 0 & 0 & 0 & 1 & 0 & 0 \\ 0 & 0 & 0 & 0 & 1 & 0 \\ 0 & 0 & 0 & 0 & 0 & 1 \\ -1 & 0 & 0 & 0 & 0 & 0 \\ 0 & -1 & 0 & 0 & 0 & 0 \\ 0 & 0 & -1 & 0 & 0 & 0 \end{bmatrix} \begin{pmatrix} \delta_w H \\ \delta_{\theta,x} H \\ \delta_{\theta,y} H \\ \delta_{p_w} H \\ \delta_{p_{\theta,x}} H \\ \delta_{p_{\theta,y}} H \end{pmatrix},
\tag{49}
$$

where p_w is the linear momentum and $p_{\theta,x}, p_{\theta,y}$ are the angular momenta.

4. Discretization of the Mindlin plate using a Partitioned Finite Element Method

The Partitioned Finite Element Method (PFEM) [22] consists of putting the system into weak form first and of applying the integration by parts on a subset of the overall system second. For the Mindlin plate the integration by parts can be applied to first two lines of system (41). This choice will make appear the momenta and forces at the boundary as control inputs. Alternatively, the last two of (41) could have been selected to perform the integration by parts. In this latter case the linear and angular velocities at the boundary would appear as control inputs. Keeping this in mind, the most suitable choice will depend on the physical problem under consideration.

4.1. Weak form

The test functions are of scalar, vectorial and tensorial nature. Keeping the same notation as in section 3, the scalar test function is denoted by v_w, the vectorial one by $\boldsymbol{v}_\theta$, $\boldsymbol{v}_\gamma$ the tensorial one by $\mathbb{V}_\kappa$.

4.1.1. Boundary control through forces and momenta

The first line of (41) is multiplied by v_w (multiplication by a scalar), the second line and the fourth by $\boldsymbol{v}_\theta$, $\boldsymbol{v}_\gamma$ (scalar product of $\mathbb{R}^2$) and the third one by $\mathbb{V}_\kappa$ (tensor contraction):

$$
\int_\Omega v_w \frac{\partial \alpha_w}{\partial t} \, \mathrm{d}\Omega = \int_\Omega v_w \mathrm{div}(\boldsymbol{e}_\gamma) \, \mathrm{d}\Omega,
\tag{50}
$$

$$
\int_\Omega \boldsymbol{v}_\theta \cdot \frac{\partial \boldsymbol{\alpha}_\theta}{\partial t} \, \mathrm{d}\Omega = \int_\Omega \boldsymbol{v}_\theta \cdot (\mathrm{Div}(\mathbb{E}_\kappa) + \boldsymbol{e}_\gamma) \, \mathrm{d}\Omega,
\tag{51}
$$

$$
\int_\Omega \mathbb{V}_\kappa : \frac{\partial \mathbb{A}_\kappa}{\partial t} \, \mathrm{d}\Omega = \int_\Omega \mathbb{V}_\kappa : \mathrm{Grad}(\boldsymbol{e}_\theta) \, \mathrm{d}\Omega,
\tag{52}
$$

$$
\int_\Omega \boldsymbol{v}_\gamma \cdot \frac{\partial \boldsymbol{\alpha}_\gamma}{\partial t} \, \mathrm{d}\Omega = \int_\Omega \boldsymbol{v}_\gamma \cdot (\mathrm{grad}(e_w) - \boldsymbol{e}_\theta) \, \mathrm{d}\Omega.
\tag{53}
$$

The right-hand side of equation (50) has to be integrated by parts

$$
\int_\Omega v_w \mathrm{div}(\boldsymbol{e}_\gamma) \, \mathrm{d}\Omega = \int_{\partial\Omega} v_w \underbrace{\boldsymbol{n} \cdot \boldsymbol{e}_\gamma}_{q_n} \, \mathrm{d}s - \int_\Omega \mathrm{grad}(v_w) \cdot \boldsymbol{e}_\gamma \, \mathrm{d}\Omega,
\tag{54}
$$

15

as well as the right-hand side of equation (51)

$$\int_\Omega \boldsymbol{v}_\theta \cdot (\mathrm{Div}(\mathbb{E}_\kappa) + \boldsymbol{e}_\gamma) \; \mathrm{d}\Omega = \int_{\partial\Omega} \boldsymbol{v}_\theta \cdot (\boldsymbol{n} \cdot \mathbb{E}_\kappa) \; \mathrm{d}s - \int_\Omega \{\mathrm{Grad}(\boldsymbol{v}_\theta) : \mathbb{E}_\kappa - \boldsymbol{v}_\theta \cdot \boldsymbol{e}_\gamma\} \; \mathrm{d}\Omega. \quad (55)$$

The usual additional manipulation is performed on the boundary term containing the momenta, so that the proper boundary values arise:

$$\int_{\partial\Omega} \boldsymbol{v}_\theta \cdot (\boldsymbol{n} \cdot \mathbb{E}_\kappa) \; \mathrm{d}s = \int_{\partial\Omega} \{(\boldsymbol{v}_\theta \cdot \boldsymbol{n})\boldsymbol{n} + (\boldsymbol{v}_\theta \cdot \boldsymbol{s})\boldsymbol{s}\} \cdot (\boldsymbol{n} \cdot \mathbb{E}_\kappa) \; \mathrm{d}s$$
$$= \int_{\partial\Omega} \{v_{\omega_n} M_{nn} + v_{\omega_s} M_{ns}\} \; \mathrm{d}s. \quad (56)$$

So defining $v_{\omega_n} := \boldsymbol{v}_\theta \cdot \boldsymbol{n}$ and $v_{\omega_s} := \boldsymbol{v}_\theta \cdot \boldsymbol{s}$ the final weak form obtained from system (41) reads:

$$\begin{cases} \displaystyle\int_\Omega v_w \frac{\partial \alpha_w}{\partial t} \; \mathrm{d}\Omega & = -\displaystyle\int_\Omega \mathrm{grad}(v_w) \cdot \boldsymbol{e}_\gamma \; \mathrm{d}\Omega + \displaystyle\int_{\partial\Omega} v_w q_n \; \mathrm{d}s, \\[12pt] \displaystyle\int_\Omega \boldsymbol{v}_\theta \cdot \frac{\partial \boldsymbol{\alpha}_\theta}{\partial t} \; \mathrm{d}\Omega & = -\displaystyle\int_\Omega \{\mathrm{Grad}(\boldsymbol{v}_\theta) : \mathbb{E}_\kappa - \boldsymbol{v}_\theta \cdot \boldsymbol{e}_\gamma\} \; \mathrm{d}\Omega + \displaystyle\int_{\partial\Omega} \{v_{\omega_n} M_{nn} + v_{\omega_s} M_{ns}\} \; \mathrm{d}s, \\[12pt] \displaystyle\int_\Omega \mathbb{V}_\kappa : \frac{\partial \mathbb{A}_\kappa}{\partial t} \; \mathrm{d}\Omega & = \displaystyle\int_\Omega \mathbb{V}_\kappa : \mathrm{Grad}(\boldsymbol{e}_\theta) \; \mathrm{d}\Omega, \\[12pt] \displaystyle\int_\Omega \boldsymbol{v}_\gamma \cdot \frac{\partial \boldsymbol{\alpha}_\gamma}{\partial t} \; \mathrm{d}\Omega & = \displaystyle\int_\Omega \boldsymbol{v}_\gamma \cdot (\mathrm{grad}(e_w) - \boldsymbol{e}_\theta) \; \mathrm{d}\Omega. \end{cases}$$
$$(57)$$

In this first case, the boundary controls $\boldsymbol{u}_\partial$ and the corresponding output $\boldsymbol{y}_\partial$ are:

$$\boldsymbol{u}_\partial = \begin{pmatrix} q_n \\ M_{nn} \\ M_{ns} \end{pmatrix}_{\partial\Omega}, \qquad \boldsymbol{y}_\partial = \begin{pmatrix} w_t \\ \omega_n \\ \omega_s \end{pmatrix}_{\partial\Omega}.$$

4.1.2. Boundary control through kinematic variables

Alternatively, in this second case, the same procedure can be performed on the two last lines of the system written in weak form (equations (52), (53)). Once the due calculations are carried out, it is found:

$$\begin{cases} \displaystyle\int_\Omega v_w \frac{\partial \alpha_w}{\partial t} \; \mathrm{d}\Omega & = \displaystyle\int_\Omega v_w \mathrm{div}(\boldsymbol{e}_\gamma) \; \mathrm{d}\Omega, \\[12pt] \displaystyle\int_\Omega \boldsymbol{v}_\theta \cdot \frac{\partial \boldsymbol{\alpha}_\theta}{\partial t} \; \mathrm{d}\Omega & = \displaystyle\int_\Omega \boldsymbol{v}_\theta \cdot (\mathrm{Div}(\mathbb{E}_\kappa) + \boldsymbol{e}_\gamma) \; \mathrm{d}\Omega, \\[12pt] \displaystyle\int_\Omega \mathbb{V}_\kappa : \frac{\partial \mathbb{A}_\kappa}{\partial t} \; \mathrm{d}\Omega & = -\displaystyle\int_\Omega \mathrm{Div}(\mathbb{V}_\kappa) \cdot \boldsymbol{e}_\theta \; \mathrm{d}\Omega + \displaystyle\int_{\partial\Omega} \{v_{M_{nn}} \omega_n + v_{M_{ns}} \omega_s\} \; \mathrm{d}s, \\[12pt] \displaystyle\int_\Omega \boldsymbol{v}_\gamma \cdot \frac{\partial \boldsymbol{\alpha}_\gamma}{\partial t} \; \mathrm{d}\Omega & = -\displaystyle\int_\Omega \{\mathrm{div}(\boldsymbol{v}_\gamma)e_w + \boldsymbol{v}_\gamma \cdot \boldsymbol{e}_\theta\} \; \mathrm{d}\Omega + \displaystyle\int_{\partial\Omega} v_{q_n} w_t \; \mathrm{d}s, \end{cases}$$
$$(58)$$

where $v_{M_{nn}} = \mathbb{V}_\kappa : (\boldsymbol{n} \otimes \boldsymbol{n})$, $v_{M_{ns}} = \mathbb{V}_\kappa : (\boldsymbol{s} \otimes \boldsymbol{n})$ and $v_{q_n} = \boldsymbol{v}_\gamma \cdot \boldsymbol{n}$. In this second case, the boundary controls $\boldsymbol{u}_\partial$ and corresponding output $\boldsymbol{y}_\partial$ are:

$$\boldsymbol{u}_\partial = \begin{pmatrix} w_t \\ \omega_n \\ \omega_s \end{pmatrix}_{\partial\Omega}, \qquad \boldsymbol{y}_\partial = \begin{pmatrix} q_n \\ M_{nn} \\ M_{ns} \end{pmatrix}_{\partial\Omega}.$$

4.2. Finite-dimensional port-Hamiltonian system

In this section the formulation (57) is used is order to explain the discretization procedure. Test and co-energy variables are discretized using the same basis functions (Galerkin Method):

$$
\begin{aligned}
v_w &= \sum_{i=1}^{N_w} \phi_w^i(x,y)\, v_w^i, & e_w &= \sum_{i=1}^{N_w} \phi_w^i(x,y)\, e_w^i(t), \\
\boldsymbol{v}_\theta &= \sum_{i=1}^{N_\theta} \boldsymbol{\phi}_\theta^i(x,y)\, v_\theta^i, & \boldsymbol{e}_\theta &= \sum_{i=1}^{N_\theta} \boldsymbol{\phi}_\theta^i(x,y)\, e_\theta^i(t), \\
\mathbb{V}_\kappa &= \sum_{i=1}^{N_\kappa} \boldsymbol{\Phi}_\kappa^i(x,y)\, v_\kappa^i, & \mathbb{E}_\kappa &= \sum_{i=1}^{N_\kappa} \boldsymbol{\Phi}_\kappa^i(x,y)\, e_\kappa^i(t), \\
\boldsymbol{v}_\gamma &= \sum_{i=1}^{N_\gamma} \boldsymbol{\phi}_\gamma^i(x,y)\, v_\gamma^i, & \boldsymbol{e}_\gamma &= \sum_{i=1}^{N_\gamma} \boldsymbol{\phi}_\gamma^i(x,y)\, e_\gamma^i(t).
\end{aligned}
\tag{59}
$$

The basis functions ϕ_w^i, $\boldsymbol{\phi}_\theta^i$, $\boldsymbol{\Phi}_\kappa^i$, $\boldsymbol{\phi}_\gamma^i$ have to be chosen in a suitable function space $\mathcal{V}^h$ in the domain of operator J, defined in (41), i.e. $\mathcal{V}^h \subset \mathcal{V} \in \mathcal{D}(J)$. This will be discussed in section 5. The discretized skew-symmetric bilinear form on the right-hand side of (57) then becomes:

$$
\boldsymbol{J}_d = \begin{bmatrix}
0 & 0 & 0 & -\boldsymbol{D}_{\mathrm{grad}}^T \\
0 & 0 & -\boldsymbol{D}_{\mathrm{Grad}}^T & -\boldsymbol{D}_0^T \\
0 & \boldsymbol{D}_{\mathrm{Grad}} & 0 & 0 \\
\boldsymbol{D}_{\mathrm{grad}} & \boldsymbol{D}_0 & 0 & 0
\end{bmatrix},
\tag{60}
$$

where the matrices are computed in the following way:

$$
\begin{aligned}
\boldsymbol{D}_{\mathrm{Grad}}(i,j) &= \int_\Omega \boldsymbol{\Phi}_\kappa^i : \mathrm{Grad}(\boldsymbol{\phi}_\theta^j)\, \mathrm{d}\Omega, & &\in \mathbb{R}^{N_\kappa \times N_\theta}, \\
\boldsymbol{D}_{\mathrm{grad}}(i,j) &= \int_\Omega \boldsymbol{\phi}_\gamma^i \cdot \mathrm{grad}(\phi_w^j)\, \mathrm{d}\Omega, & &\in \mathbb{R}^{N_\gamma \times N_w}, \\
\boldsymbol{D}_0(i,j) &= -\int_\Omega \boldsymbol{\phi}_\gamma^i \cdot \boldsymbol{\phi}_\theta^j\, \mathrm{d}\Omega, & &\in \mathbb{R}^{N_\gamma \times N_\theta}.
\end{aligned}
\tag{61}
$$

The notation $\boldsymbol{D}(i,j)$ indicates the entry in matrix $\boldsymbol{D}$ corresponding to the ith row and jth column. The energy variables are deduced from the co-energy variables:

$$
\begin{aligned}
\alpha_w &= \rho h e_w, & \mathbb{A}_\kappa &= \mathbb{D}^{-1}\mathbb{E}_\kappa, \\
\boldsymbol{\alpha}_\theta &= \frac{\rho h^3}{12} \boldsymbol{e}_\theta, & \boldsymbol{\alpha}_\gamma &= \frac{1}{Ghk} \boldsymbol{e}_\gamma.
\end{aligned}
\tag{62}
$$

The symmetric bilinear form on the left-hand side of (57) is discretized as:

$$
\boldsymbol{M} = \mathrm{diag}[\boldsymbol{M}_w,\ \boldsymbol{M}_\theta,\ \boldsymbol{M}_\kappa,\ \boldsymbol{M}_\gamma], \quad \text{with}
$$

$$
\begin{aligned}
\boldsymbol{M}_w(i,j) &= \int_\Omega \rho h\, \phi_w^i\, \phi_w^j\, \mathrm{d}\Omega, \in \mathbb{R}^{N_w \times N_w}, & \boldsymbol{M}_\kappa(i,j) &= \int_\Omega \left(\mathbb{D}^{-1}\boldsymbol{\Phi}_\kappa^i\right) : \boldsymbol{\Phi}_\kappa^j\, \mathrm{d}\Omega, \in \mathbb{R}^{N_\kappa \times N_\kappa}, \\
\boldsymbol{M}_\theta(i,j) &= \int_\Omega \frac{\rho h^3}{12} \boldsymbol{\phi}_\theta^i \cdot \boldsymbol{\phi}_\theta^j\, \mathrm{d}\Omega, \in \mathbb{R}^{N_\theta \times N_\theta}, & \boldsymbol{M}_\gamma(i,j) &= \int_\Omega \frac{1}{Ghk} \boldsymbol{\phi}_\gamma^i \cdot \boldsymbol{\phi}_\gamma^j\, \mathrm{d}\Omega, \in \mathbb{R}^{N_\gamma \times N_\gamma}.
\end{aligned}
\tag{63}
$$

The boundary variables are then discretized as:

$$q_n = \sum_{i=1}^{N_{q_n}} \phi_{q_n}^i(s) q_n^i, \qquad M_{nn} = \sum_{i=1}^{N_{M_{nn}}} \phi_{M_{nn}}^i(s) M_{nn}^i, \qquad M_{ns} = \sum_{i=1}^{N_{M_{ns}}} \phi_{M_{ns}}^i(s) M_{ns}^i. \qquad (64)$$

The variables are defined only over the boundary $\partial\Omega$. Consequently, the input matrix reads:

$$\boldsymbol{B} = \begin{bmatrix} \boldsymbol{B}_{q_n} & 0 & 0 \\ 0 & \boldsymbol{B}_{M_{nn}} & \boldsymbol{B}_{M_{ns}} \\ 0 & 0 & 0 \\ 0 & 0 & 0 \end{bmatrix}. \qquad (65)$$

The inner components are computed as:

$$\begin{aligned}
\boldsymbol{B}_{q_n}(i,j) &= \int_{\partial\Omega} \phi_w^i\, \phi_{q_n}^j \,\mathrm{d}s, \quad \in \mathbb{R}^{N_w \times N_{q_n}}, \\
\boldsymbol{B}_{M_{nn}}(i,j) &= \int_{\partial\Omega} (\boldsymbol{\phi}_\theta^i \cdot \boldsymbol{n})\, \phi_{M_{nn}}^j \,\mathrm{d}s, \quad \in \mathbb{R}^{N_w \times N_{M_{nn}}}, \\
\boldsymbol{B}_{M_{ns}}(i,j) &= \int_{\partial\Omega} (\boldsymbol{\phi}_\theta^i \cdot \boldsymbol{s})\, \phi_{M_{ns}}^j \,\mathrm{d}s, \quad \in \mathbb{R}^{N_w \times N_{M_{ns}}}.
\end{aligned} \qquad (66)$$

The final port-Hamiltonian system (as defined in [24], where the presence of a mass matrix $\boldsymbol{M}$ is taken into account) is written as:

$$\begin{aligned}
\boldsymbol{M}\dot{\boldsymbol{e}} &= \boldsymbol{J}_d\,\boldsymbol{e} + \boldsymbol{B}\,\boldsymbol{u}_\partial, \\
\boldsymbol{y}_\partial &= \boldsymbol{B}^T\,\boldsymbol{e},
\end{aligned} \qquad (67)$$

where $\boldsymbol{e} = \left(e_w^1, \cdots, e_\gamma^{N_\gamma} \right)^T$ and $\boldsymbol{u}_\partial = \left(q_n^1, \ldots, M_{ns}^{N_{M_{ns}}} \right)^T$ are the concatenations of the degrees of freedom for the different variables. The discrete Hamiltonian is then found as:

$$\begin{aligned}
H_d &= \frac{1}{2} \int_\Omega \{ \alpha_w e_w + \boldsymbol{\alpha}_\theta \cdot \boldsymbol{e}_\theta + \mathbb{A}_\kappa : \mathbb{E}_\kappa + \boldsymbol{\alpha}_\gamma \cdot \boldsymbol{e}_\gamma \} \,\mathrm{d}\Omega \\
&= \frac{1}{2} \left\{ \boldsymbol{e}_w^T\, \boldsymbol{M}_w\, \boldsymbol{e}_w + \boldsymbol{e}_\theta^T\, \boldsymbol{M}_\theta\, \boldsymbol{e}_\theta + \boldsymbol{e}_\kappa^T\, \boldsymbol{M}_\kappa\, \boldsymbol{e}_\kappa + \boldsymbol{e}_\gamma^T\, \boldsymbol{M}_\gamma\, \boldsymbol{e}_\gamma \right\} \\
&= \frac{1}{2}\, \boldsymbol{e}^T \boldsymbol{M} \boldsymbol{e}.
\end{aligned} \qquad (68)$$

Then it naturally follows that:

$$\dot{H}_d = \boldsymbol{y}_\partial^T \boldsymbol{u}_\partial. \qquad (69)$$

This is equivalent to the energy balance of the continuous system, expressed by equation (42). Definition (68), together with system (67) are the finite-dimensional equivalent of (37) and (41). Again, the discretized system obtained via PFEM shares the same properties as those of the original infinite-dimensional system, the discretization method is therefore structure-preserving.
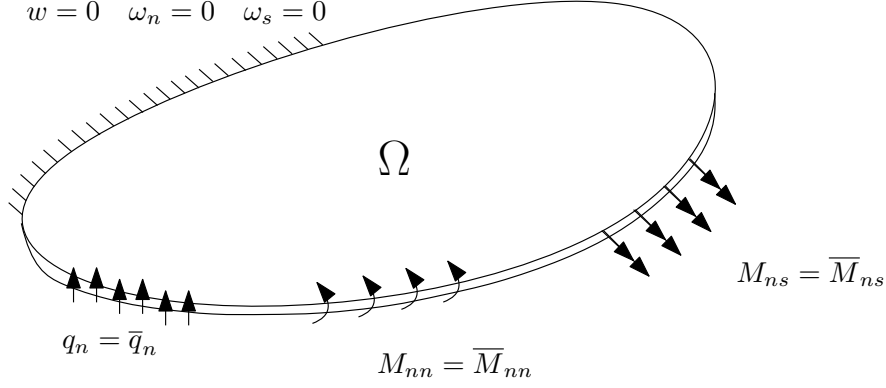
Figure 3: Clamped plate with distributed shear forces and torsional and flexural momenta at the border.

4.3. Mixed boundary conditions

This formulation provides as control term the dynamic variables at the boundary, namely forces and momenta, whereas the kinematic variables do not appear. In order to handle mixed boundary conditions, i.e. a clamped or a simply supported plate with free or loaded edges (see Fig. 3), the boundary control term has to be split into known and unknown variables, i.e. given boundary conditions and reactions at the boundaries respectively. These terms may be rearranged by introducing a permutation matrix P. The control term may be rewritten in the following way:

$$\boldsymbol{u}_\partial = \boldsymbol{B}\boldsymbol{P}\begin{pmatrix}\boldsymbol{f}\\\boldsymbol{\lambda}\end{pmatrix} = \boldsymbol{B}\begin{bmatrix}\boldsymbol{P}_f & \boldsymbol{P}_\lambda\end{bmatrix}\begin{pmatrix}\boldsymbol{f}\\\boldsymbol{\lambda}\end{pmatrix}. \tag{70}$$

Equivalently the boundary outputs can be split. The terms corresponding to $\boldsymbol{\lambda}$ will be the kinematic variables set by the boundary conditions. The term corresponding to $\boldsymbol{f}$ are the kinematic variables at the controlled boundaries. The following equation allows splitting up the outputs into these two contributions:

$$\boldsymbol{y}_\partial = \boldsymbol{P}\begin{pmatrix}\boldsymbol{y}_f\\\boldsymbol{y}_\lambda\end{pmatrix} = \begin{bmatrix}\boldsymbol{P}_f & \boldsymbol{P}_\lambda\end{bmatrix}\begin{pmatrix}\boldsymbol{y}_f\\\boldsymbol{y}_\lambda\end{pmatrix}. \tag{71}$$

So that the output equation becomes:

$$\begin{pmatrix}\boldsymbol{y}_f\\\boldsymbol{y}_\lambda\end{pmatrix} = \begin{bmatrix}\boldsymbol{P}_f^T\\\boldsymbol{P}_\lambda^T\end{bmatrix}\boldsymbol{B}^T\boldsymbol{e}. \tag{72}$$

The port-Hamiltonian finite-dimensional system is rewritten equivalently by highlighting the known control terms, the Lagrange multipliers (reactions at the boundary) and the constraints, arising from the fact that the function $\boldsymbol{y}_\lambda$ is known. In case of a homogenous Dirichlet condition, i.e. $\boldsymbol{y}_\lambda = 0$, it is obtained:

$$\begin{bmatrix}\boldsymbol{M} & 0\\0 & 0\end{bmatrix}\frac{\mathrm{d}}{\mathrm{d}t}\begin{pmatrix}\boldsymbol{e}\\\boldsymbol{\lambda}\end{pmatrix} = \begin{bmatrix}\boldsymbol{J}_d & \boldsymbol{B}\boldsymbol{P}_\lambda\\-\boldsymbol{P}_\lambda^T\boldsymbol{B}^T & 0\end{bmatrix}\begin{pmatrix}\boldsymbol{e}\\\boldsymbol{\lambda}\end{pmatrix} + \begin{bmatrix}\boldsymbol{B}\boldsymbol{P}_f\\0\end{bmatrix}\boldsymbol{f},$$
$$\boldsymbol{y}_f = \begin{bmatrix}\boldsymbol{P}_f^T\boldsymbol{B}^T & 0\end{bmatrix}\begin{pmatrix}\boldsymbol{e}\\\boldsymbol{\lambda}\end{pmatrix}. \tag{73}$$

This differential-algebraic port-Hamiltonian system can be treated applying results detailed in [23, 24].

5. Numerical studies

In this section, the consistency of the proposed model is illustrated numerically. For this purpose the computation of the eigenvalues of a square plate and time-domain simulations for several boundary conditions are presented. The formulation used in the numerical implementation is the one presented in section 4.2.

5.1. Finite Element Choice

The domain of the operator J in (41) is

$$\mathcal{D}(J) = H^1(\Omega) \times H^1(\Omega, \mathbb{R}^2) \times H^{\mathrm{Div}}(\Omega, \mathbb{R}^{2\times2}_{\mathrm{sym}}) \times H^{\mathrm{div}}(\Omega, \mathbb{R}^2) \quad \text{and boundary conditions.}$$

For this reason a suitable choice for the functional space is:

$$(v_w, \boldsymbol{v}_\theta, \mathbb{V}_\kappa, \boldsymbol{v}_\gamma) \in H^1(\Omega) \times H^1(\Omega, \mathbb{R}^2) \times H^1(\Omega, \mathbb{R}^{2\times2}_{\mathrm{sym}}) \times H^1(\Omega, \mathbb{R}^2) \equiv \mathscr{H}, \qquad (74)$$

since $\mathscr{H} \subset \mathcal{D}(J)$. Then, for the Finite Element choice, denote:

$$H^1_r(\mathbb{P}_l) = \{v \in H^1(\Omega) |\ v_{|T} \in \mathbb{P}_l\ \forall T \in \mathbb{T}_r\}$$

the finite element space which is a subspace of $H^1(\Omega)$, based on the shape function space of piecewise polynomials of degree l. The shape function space is defined over the mesh $\mathbb{T}_r = \bigcup_i T_i$, where the cells T_i are triangles. These spaces can be scalar-valued, vector-valued or symmetric tensor-valued, depending on the variables to be discretized. The parameter r is the average size of a mesh element. In the following all the co-energy variables $\boldsymbol{e}$ are discretized by the same finite element space. The analysis were conducted using two different finite element spaces:

1. the first order Lagrange polynomials $H^1_r(\mathbb{P}_1)$;
2. the second order Lagrange polynomials $H^1_r(\mathbb{P}_2)$.

The Lagrange multipliers $\boldsymbol{\lambda}$ are discretized by using Lagrange polynomials defined over the boundary. The order of the Lagrange polynomials is the same as the one chosen for the co-energy variable. The corresponding finite element is denoted by $H^1_r(\mathbb{P}_l, \partial\Omega)$

Remark 4. *The selected finite element are conforming as they discretized space $\mathscr{H} \subset \mathcal{D}(J)$. Nevertheless, this choice is not the less computationally expensive as conforming elements are defined by the larger set $\mathcal{D}(J)$. Anyway due to the lack of Arnold-Winther elements [33] (that discretizes the space $H^{\mathrm{Div}}(\Omega, \mathbb{R}^{2\times2}_{\mathrm{sym}})$) in FEniCS library (or in any other standard library), this is the best available option for numerical computations.*

5.2. Eigenvalues Computation

The test case for this analysis is a simple square plate of side L, a benchmark problem which has been studied in [34, 35, 36] for different boundary conditions:

- all clamped CCCC, i.e. $w_t = 0$, $\omega_n = 0$, $\omega_s = 0$;

- simply supported hard SSSS, i.e. $w_t = 0$, $M_{nn} = 0$, $\omega_s = 0$;

- half-clamped half-simply supported SCSC;

<div align="center">20</div>

- all clamped but one side free CCCF (for the free condition it holds $q_n = 0$, $M_{nn} = 0$, $M_{ns} = 0$).

Two different thickness to length ratios h/L are considered: $h/L = 0.1$ representative of a thick plate and $h/L = 0.01$ representative of a thin plate. In order to compare our results with [34], the frequencies ω_{mn}^h are computed in the following non-dimensional form:

$$\widehat{\omega}_{mn}^h = \omega_{mn}^h L \left(\frac{2(1+\nu)\rho}{E} \right)^{1/2},$$

m and n being the numbers of half-waves occurring in the mode shapes in the x and y directions, respectively. The only parameters which influence the results are Poisson's ratio $\nu = 0.3$, the correction factor k, whose value is taken equal to $k = 0.8601$ for CCCC and CCCF, $k = 0.8333$ for SSSS, $k = 0.822$ for SCSC (for comparison purposes) and the thickness-to-span ratio h/L. The reported non-dimensional frequencies are independent of the remaining geometrical and physical parameters. The error is computed as:

$$\varepsilon = \frac{\mathrm{abs}(\widehat{\omega}_{mn}^h - \omega_{mn}^{DR})}{\omega_{mn}^{DR}},$$

where ω_{mn}^{DR} are the eigenvalues calculated in [34] using an analytical procedure. The results obtained using $H_r^1(\mathbb{P}_1), H_r^1(\mathbb{P}_2)$ for the thick and thin case are reported in Tables 1, 2 respectively, together with the results from [34] (D-R) and [35] (H-H). For linear polynomials the mesh consists of a regular grid with 10 and 20 elements by side. For quadratic polynomials the mesh consists of a regular grid with 5 and 10 elements by side. Ten elements in $H_r^1(\mathbb{P}_1)$ and 5 in $H_r^1(\mathbb{P}_2)$ have the same number of degree of freedom $n = 968$. Analogously, 20 elements in $H_r^1(\mathbb{P}_1)$ and 10 in $H_r^1(\mathbb{P}_2)$ have the same degree of freedom $n = 3528$. In the thick plate case, the error is limited to 2% in each for any choice of the finite element space. On the contrary the thin case exhibits worse results, particularly for the polynomials of order 1. This must be linked to the shear locking phenomenon since $\boldsymbol{M}_w \propto h$, $\boldsymbol{M}_\theta \propto h^3$, $\boldsymbol{M}_\kappa \propto h^{-3}$ and $\boldsymbol{M}_\gamma \propto h^{-1}$. Higher order elements (like the second order Lagrange polynomials $\mathbb{P}_2$) allow alleviating the problem, but this issue is still present with very thin plate as the results worsen when the thickness to length ratio decreases to $h/L = 0.01$. Anyway, the computed eigenvalues are consistent with those obtained with other methods. The first four eigenvectors for the different cases are reported as well (see Fig. 4 to 7).

5.3. Time-domain Simulations

In this analysis, a square plate, subject either to a non null shear force on the boundaries, either to a distributed force over the domain is considered. The physical parameters and simulation settings are reported in Table 3. Ten elements for each side and second order Lagrange polynomials are used. The symplectic Störmer-Verlet time integrator is employed, so that when no solicitation is applied to the system, the the symplectic structure is preserved. Two different simulations with different boundary conditions are considered. The initial conditions are set to zero for each variable. For the first simulation, a cantilever plate subject to gravity is considered. In order to add gravity the corresponding functional has to be discretized:

$$\boldsymbol{f}_{\text{gravity}} = - \int_\Omega v_w \rho h g \, \mathrm{d}\Omega,$$

21

BCs	Mode	$N = 10\,(\mathbb{P}_1)$	$N = 20\,(\mathbb{P}_1)$	$N = 5\,(\mathbb{P}_2)$	$N = 10\,(\mathbb{P}_2)$	H-H	D-R
CCCC	$\widehat{\omega}_{11}$	1.5999	1.5917	1.5976	1.5914	1.591	1.594
	$\widehat{\omega}_{21}$	3.0615	3.0410	3.0584	3.0405	3.039	3.046
	$\widehat{\omega}_{12}$	3.0615	3.0410	3.0677	3.0405	3.039	3.046
	$\widehat{\omega}_{22}$	4.3161	4.2682	4.3109	4.2662	4.263	4.285
SSSS	$\widehat{\omega}_{11}$	0.9324	0.9324	0.9304	0.9302	0.930	0.930
	$\widehat{\omega}_{21}$	2.2227	2.2226	2.2223	2.2194	2.219	2.219
	$\widehat{\omega}_{12}$	2.2227	2.2226	2.2224	2.2194	2.219	2.219
	$\widehat{\omega}_{22}$	3.4142	3.3608	3.4128	3.4061	3.405	3.406
SCSC	$\widehat{\omega}_{11}$	1.3111	1.3013	1.3053	1.3004	1.300	1.302
	$\widehat{\omega}_{21}$	2.4155	2.3966	2.4040	2.3946	2.394	2.398
	$\widehat{\omega}_{12}$	2.9082	2.8871	2.9060	2.8858	2.885	2.888
	$\widehat{\omega}_{22}$	3.8906	3.8458	3.8721	3.8415	3.839	3.852
CCCF	$\widehat{\omega}_{\frac{1}{2}1}$	1.0855	1.0982	1.0845	1.0797	1.081	1.089
	$\widehat{\omega}_{\frac{3}{2}1}$	1.7636	1.7461	1.7559	1.7425	1.744	1.758
	$\widehat{\omega}_{\frac{1}{2}2}$	2.6696	2.6575	2.6762	2.6547	2.657	2.673
	$\widehat{\omega}_{\frac{5}{2}1}$	3.2248	3.1997	3.2186	3.1954	3.197	3.216

Table 1: Eigenvalues for $h/L = 0.1$ using $\mathbb{P}_1$ and $\mathbb{P}_2$:
■ reference, ■ $\varepsilon < 2\%$.

BCs	Mode	$N = 10\,(\mathbb{P}_1)$	$N = 20\,(\mathbb{P}_1)$	$N = 5\,(\mathbb{P}_2)$	$N = 10\,(\mathbb{P}_2)$	H-H	D-R
CCCC	$\widehat{\omega}_{11}$	0.1967	0.1765	0.1872	0.1762	0.1754	0.1754
	$\widehat{\omega}_{21}$	0.4030	0.3604	0.3725	0.3598	0.3574	0.3576
	$\widehat{\omega}_{12}$	0.4030	0.3604	0.4055	0.3598	0.3574	0.3576
	$\widehat{\omega}_{22}$	0.6431	0.5358	0.6043	0.5335	0.5264	0.5274
SSSS	$\widehat{\omega}_{11}$	0.1706	0.1128	0.0963	0.0963	0.0963	0.0963
	$\widehat{\omega}_{21}$	0.3576	0.2660	0.2422	0.2406	0.2406	0.2406
	$\widehat{\omega}_{12}$	0.3576	0.2660	0.2430	0.2406	0.2406	0.2406
	$\widehat{\omega}_{22}$	0.5803	0.4442	0.3874	0.3848	0.3847	0.3848
SCSC	$\widehat{\omega}_{11}$	0.1864	0.1487	0.1492	0.1418	0.1411	0.1411
	$\widehat{\omega}_{21}$	0.3649	0.2829	0.2827	0.2683	0.2668	0.2668
	$\widehat{\omega}_{12}$	0.3987	0.3485	0.3608	0.3394	0.3377	0.3377
	$\widehat{\omega}_{22}$	0.6075	0.4933	0.4940	0.4654	0.4604	0.4608
CCCF	$\widehat{\omega}_{\frac{1}{2}1}$	0.1238	0.1166	0.1197	0.1169	0.1166	0.1171
	$\widehat{\omega}_{\frac{3}{2}1}$	0.2207	0.1954	0.2092	0.1960	0.1949	0.1951
	$\widehat{\omega}_{\frac{1}{2}2}$	0.3204	0.3078	0.3188	0.3089	0.3080	0.3093
	$\widehat{\omega}_{\frac{5}{2}1}$	0.4144	0.3751	0.3938	0.3757	0.3736	0.3740

Table 2: Eigenvalues for $h/L = 0.01$ using $\mathbb{P}_1$ and $\mathbb{P}_2$:
■ reference, ■ $\varepsilon < 2\%$, ■ $\varepsilon < 5\%$, ■ $\varepsilon < 15\%$, ■ $\varepsilon < 30\%$, ■ $\varepsilon < 50\%$, ■ $\varepsilon < 80\%$.
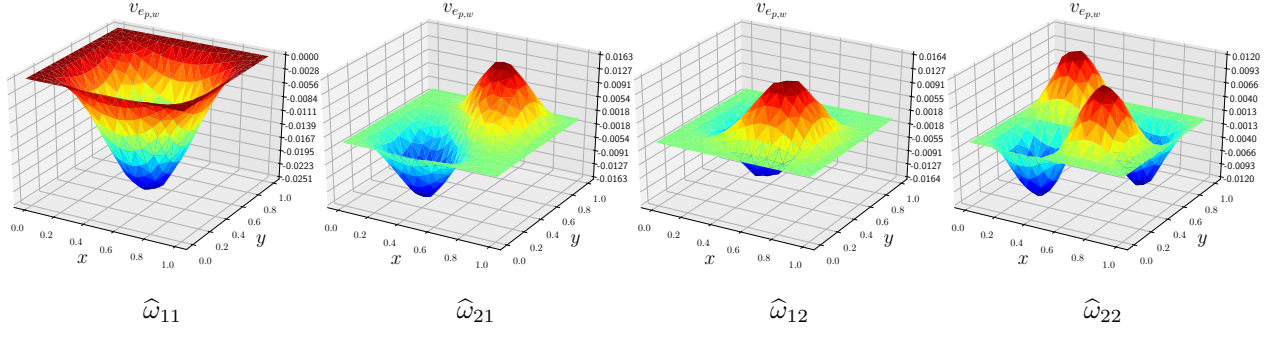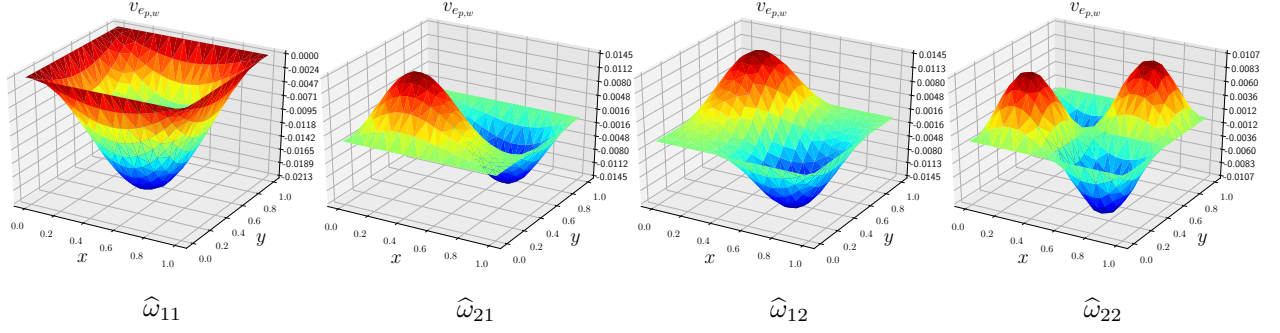
Figure 4: Eigenvectors for the CCCC case.
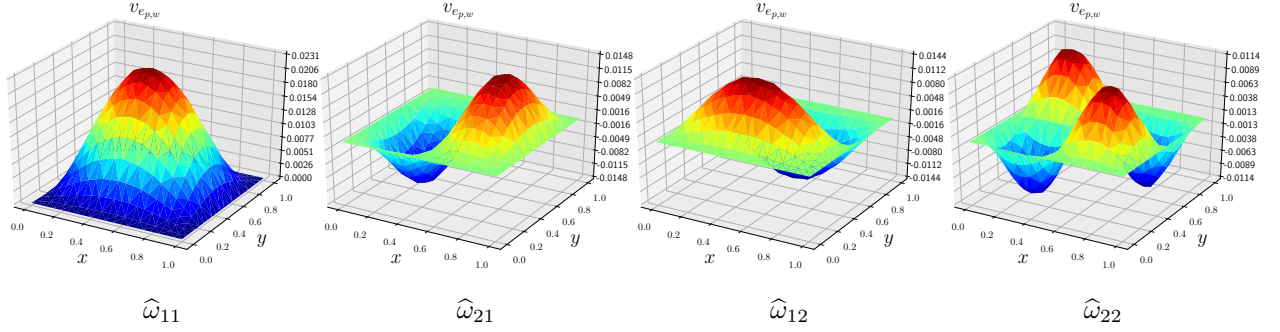

Figure 5: Eigenvectors for the SSSS case.
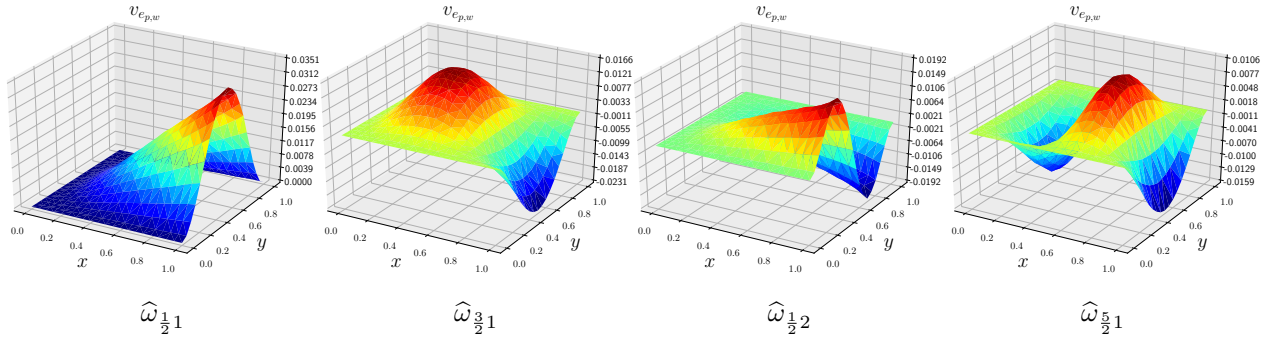

Figure 6: Eigenvectors for the SCSC case.

Figure 7: Eigenvectors for the CCCF case.

23

Plate Parameters		Simulation Settings	
E	70 $[GPa]$	Integrator	Störmer-Verlet
ρ	2700 $[kg/m^3]$	Δt	0.001 $[ms]$
ν	0.35	t_{end}	10 $[ms]$
k	5/6	N° Elements	10
h/L	0.1	FE space	$H^1_{r=L/10}(\mathbb{P}_2)$ for $\boldsymbol{e} \times H^1_{r=L/10}(\mathbb{P}_2, \partial\Omega)$ for $\boldsymbol{\lambda}$
L	1 $[m]$		

Table 3: Physical parameters and simulations settings.

(a) Simulation $n°1$
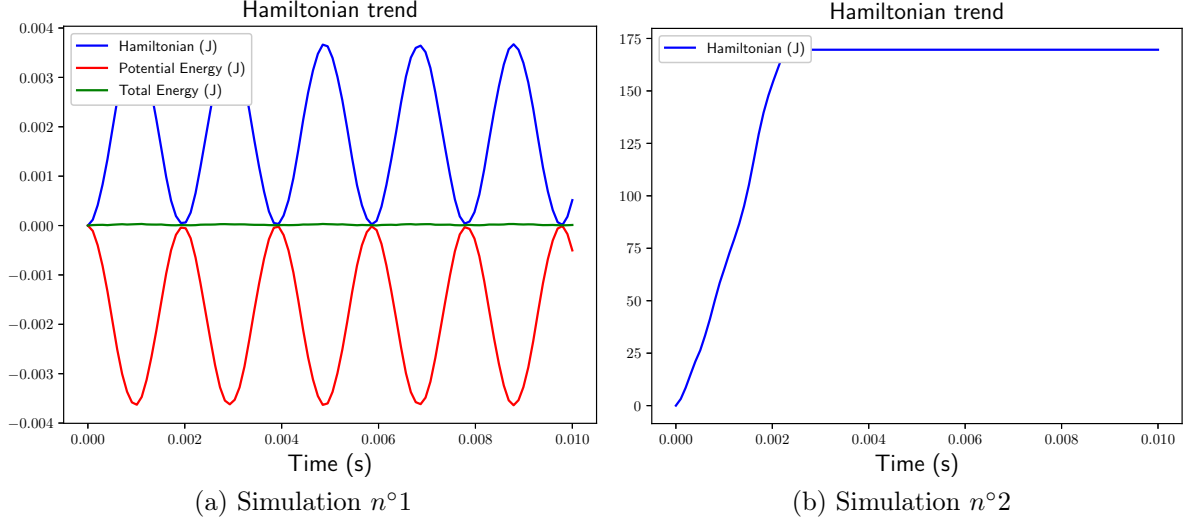
(b) Simulation $n°2$

Figure 8: Hamiltonian trend for the two simulations.

where $g = 10[m/s^2]$ is the gravity acceleration. This excitation, that applies from $t = 0$, is then simply added to the first line of system (73). For the first simulation the following boundary conditions, corresponding to the CFCF cases, are considered:

$$\text{Simulation } n° \, 1 \begin{cases} w_t = 0, \ \omega_n = \omega_s = 0, & \text{for } x = 0 \text{ and } x = 1, \\ q_n = 0, \ M_{nn} = M_{ns} = 0, & \text{for } y = 0, \\ q_n = 0, \ M_{nn} = M_{ns} = 0, & \text{for } y = 1. \end{cases}$$

Since this force admits a potential, the Hamiltonian does not correspond to the the total energy, that now includes the potential energy:

$$E_p = \int_\Omega \rho h g w \ \mathrm{d}\Omega,$$

where w is the vertical displacement field.

For the second simulation, the following boundary conditions are considered:

$$\text{Simulation } n° \, 2 \begin{cases} w_t = 0, \ \omega_n = \omega_s = 0, & \text{for } x = 0, \\ q_n = 0, \ M_{nn} = M_{ns} = 0, & \text{for } x = 1, \\ q_n = +f(x,t), \ M_{nn} = M_{ns} = 0, & \text{for } y = 0, \\ q_n = -f(x,t), \ M_{nn} = M_{ns} = 0, & \text{for } y = 1, \end{cases}$$

24

where $f(x,t)$ is the excitation defined by:

$$f(x,t) = \begin{cases} 10^5 \, \sin\left(\frac{\pi}{L}x\right) \, [Pa \cdot m], & \forall t < 0.25 \, t_{\text{end}}, \\ 0, & \forall t \geq 0.25 \, t_{\text{end}}, \end{cases}$$

t_{end} being defined in Table 3. In this case inhomogeneous boundary conditions are considered. Snapshots of the vertical displacement field are reported in Figures 9, 10. This field is obtained from the velocity field $e_w = \frac{\partial w}{\partial t}$ by applying the trapezoidal rule integration. For both simulations the output is consistent with the imposed BC and with the physical intuition of the observed phenomenon. The symplectic integration has been used to demonstrate numerically the conservation of total energy. The Hamiltonian for both simulations is reported in Figure 8. For the first one the total energy $E_t = H + E_p$ is the conserved quantity and it remains constant equal to zero as expected. For the second simulation the Hamiltonian is the conserved quantity, once the excitation is set back to zero. The conservation of energy is also obvious from Figure 10. The boundary conditions are such that the energy increases monotonically as long as the excitation is present. The deformation attained at the final time of the excitation repeats itself symmetrically with respect to axis $y = L/2$ with period given by $1/2 \, t_{\text{end}}$.

Conclusions and Perspectives

In this paper the port-Hamiltonian formulation of the Mindlin plate was enriched by the equivalent tensorial formulation and by a symplectic discretization method. The PFEM method, applied to this formulation, proves again its versatility, since it stays valid and applicable even in more complicated examples like the one presented in this article. Many features of this method and of the tensorial PH formulation are of interest:

- its capability of preserving the port-Hamiltonian structure;

- the natural derivation of boundary port-variables as inputs;

- the possibility of dealing with mixed boundary conditions inside the framework of port-Hamiltonian descriptor systems PHDAEs, detailed in [24];

- the easy implementability of the method using standard Finite Element libraries (Fenics [25] in our case);

- a coordinate free representation which makes possible to treat other planar geometries (circular, ellipsoidal, annular etc).

The formulation presented in this paper could be completed with a precise analysis of the well-posedness, in the input-output sense (as in [37] for the wave equation in $\mathbb{R}^d$). Furthermore, a proper convergence analysis is needed. Using conforming elements requires the Arnold-Winther elements. Unfortunately, these are not included inside Fenics (or in any standard library).

Another important aspect is the implementation of suitable control laws. The proposed method paves the way to the use of passivity-based approaches and of energy shaping methods. These techniques have already been largely studied in the literature [38, 39] for the
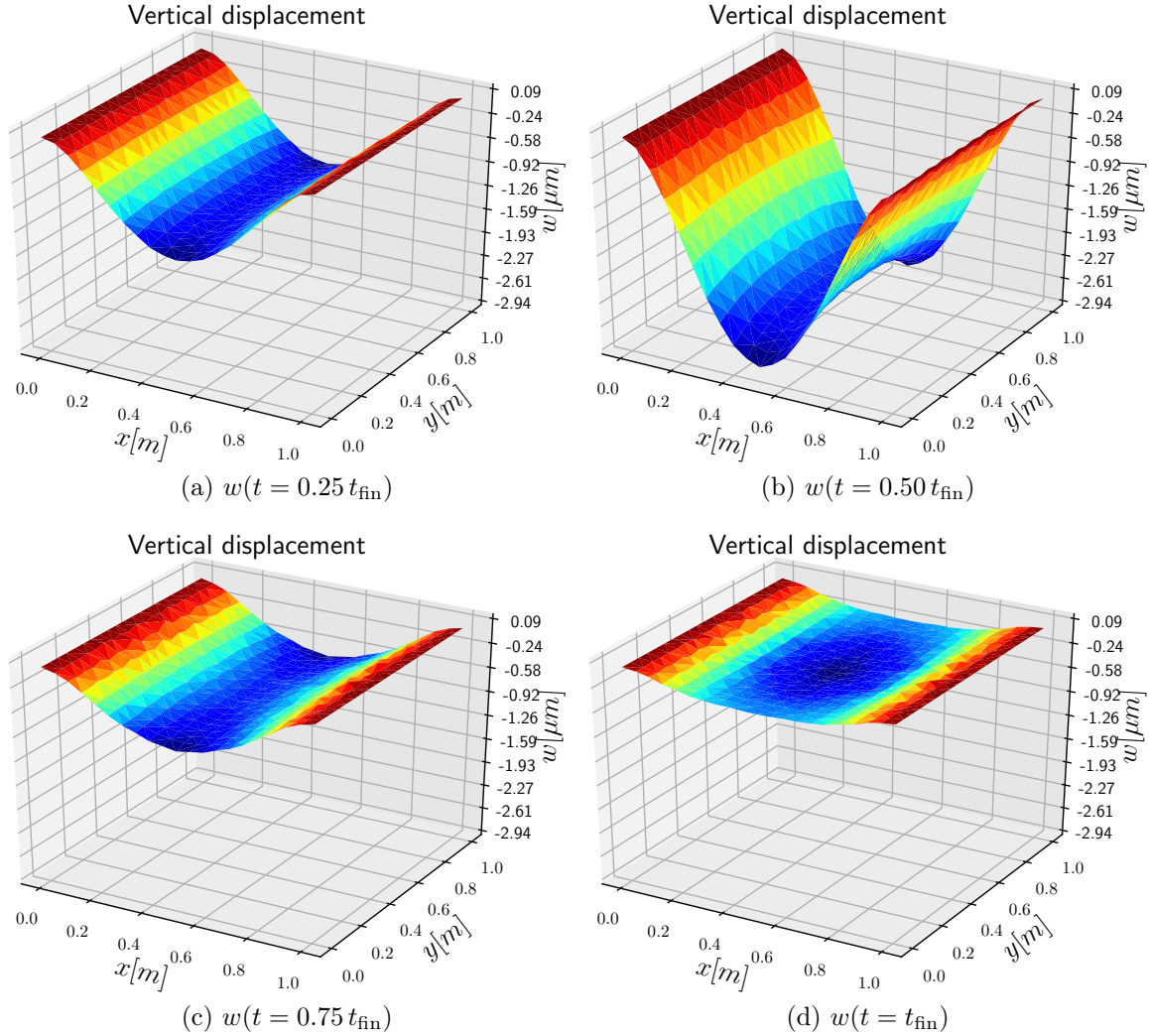
(a) $w(t = 0.25\,t_{\text{fin}})$

(b) $w(t = 0.50\,t_{\text{fin}})$

(c) $w(t = 0.75\,t_{\text{fin}})$

(d) $w(t = t_{\text{fin}})$

Figure 9: Snapshots for Simulation $n°1$.

finite-dimensional case. However, the distributed case is mainly limited to one geometrical dimension [40]. It would be of great interest, especially for control engineers, to conceive a controller able to respect given performance specifications. The port-Hamiltonian formalism and its powerfulness in modeling complex systems could be linked to standard control methodologies, already well known in the industrial field, like the LQR or H^∞ methodologies.

Acknowledgments

(a) $w(t = 0.25\,t_{\text{fin}})$

(b) $w(t = 0.50\,t_{\text{fin}})$

(c) $w(t = 0.75\,t_{\text{fin}})$

(d) $w(t = t_{\text{fin}})$
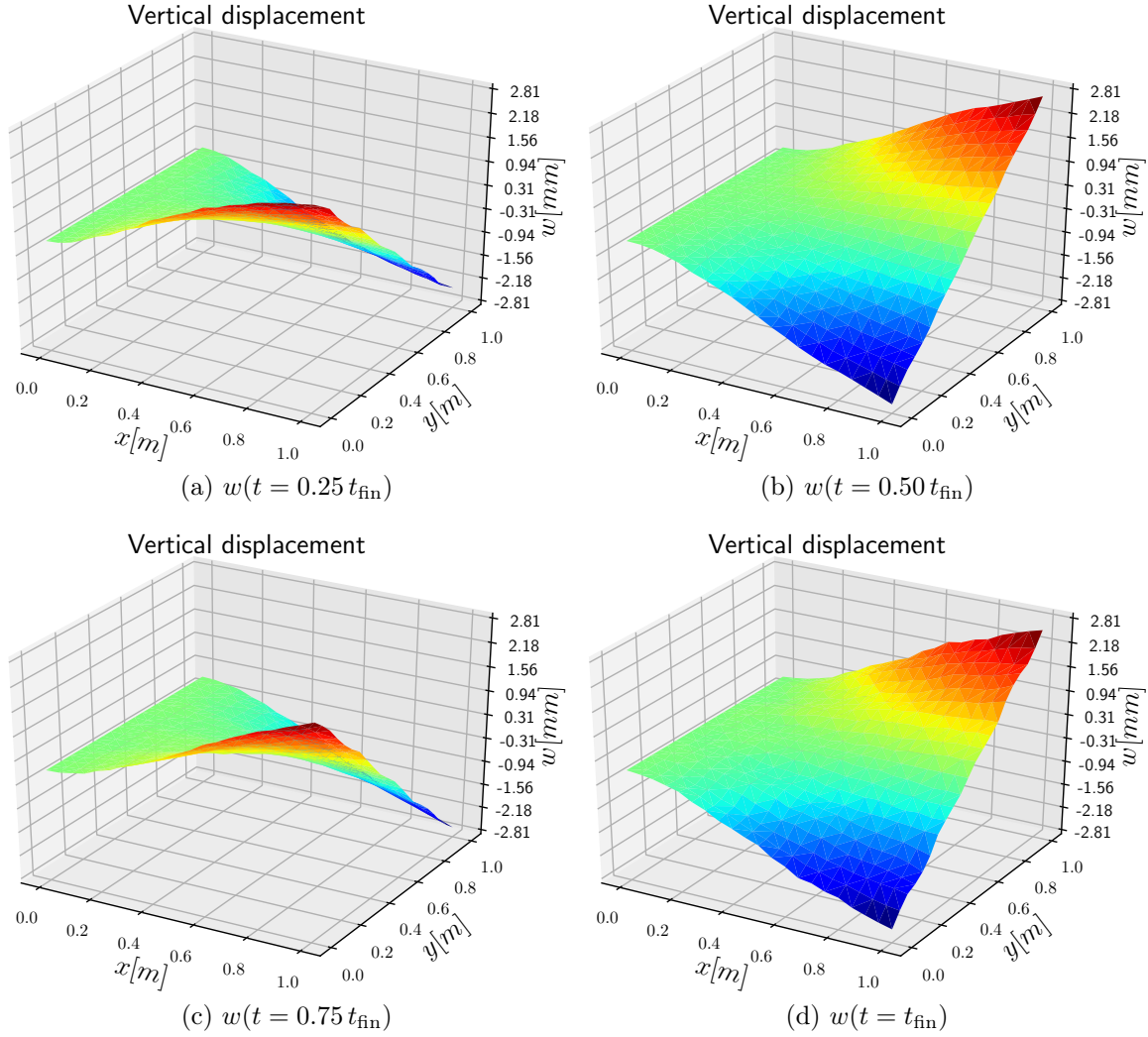
Figure 10: Snapshots for Simulation $n°2$.

References

[1] W. Yao, W. Zhong, and C. W. Lim. *Symplectic Elasticity*. WORLD SCIENTIFIC, 2009.

[2] Yao Wei-an and Sui Yong-feng. Symplectic solution system for Reissner plate bending. *Applied Mathematics and Mechanics*, 25(2):178–185, Feb 2004. https://doi.org/10.1007/BF02437319.

[3] P. J. Olver. *Applications of Lie groups to differential equations*, volume 107 of *Graduate texts in mathematics*. Springer-Verlag New York, 2 edition, 1993.

[4] Hiroaki Yoshimura and Jerrold E. Marsden. Dirac structures in lagrangian mechanics part i: Implicit lagrangian systems. *Journal of Geometry and Physics*, 57(1):133 – 156, 2006. https://doi.org/10.1016/j.geomphys.2006.02.009.

[5] Hiroaki Yoshimura and Jerrold E. Marsden. Dirac structures in lagrangian mechanics

27

part ii: Variational structures. *Journal of Geometry and Physics*, 57(1):209 – 250, 2006. https://doi.org/10.1016/j.geomphys.2006.02.012.

[6] J. Cervera, A. J. van der Schaft, and A. Baños. Interconnection of port-Hamiltonian systems and composition of dirac structures. *Automatica*, 43(2):212–225, feb 2007. https://doi.org/10.1016/j.automatica.2006.08.014.

[7] M. Kurula, H. Zwart, A. J. van der Schaft, and J. Behrndt. Dirac structures and their composition on Hilbert spaces. *Journal of mathematical analysis and applications*, 372(2):402–422, 2010. https://doi.org/10.1016/j.jmaa.2010.07.004.

[8] R. Pasumarthy and A. J. van der Schaft. On interconnections of infinite-dimensional port-Hamiltonian systems. In *Proceedings of the 16th International Symposium on Mathematical Theory of Networks and Systems (MTNS)*. Katholieke Universiteit Leuven, july 2004.

[9] A.J. van der Schaft and B. Maschke. Hamiltonian formulation of distributed-parameter systems with boundary energy flow. *Journal of Geometry and Physics*, 42(1):166 – 194, 2002. https://doi.org/10.1016/S0393-0440(01)00083-3.

[10] J.A. Villegas. *A Port-Hamiltonian Approach to Distributed Parameter Systems*. PhD thesis, University of Twente, May 2007.

[11] B. Jacob and H. Zwart. *Linear Port-Hamiltonian Systems on Infinite-dimensional Spaces*. Number 223 in Operator Theory: Advances and Applications. Springer Verlag, Germany, 2012. https://doi.org/10.1007/978-3-0348-0399-1.

[12] V. Duindam, A. Macchelli, S. Stramigioli, and H. Bruyninckx. *Modeling and Control of Complex Physical Systems*. Springer Verlag, 2009. https://doi.org/10.1007/978-3-642-03196-0.

[13] Y. Le Gorrec, H. Zwart, and B. Maschke. Dirac structures and Boundary Control Systems associated with Skew-Symmetric Differential Operators. *SIAM Journal on Control and Optimization*, 44(5):1864–1892, 2005. https://doi.org/10.1137/040611677.

[14] G. Golo, V. Talasila, A. J. van der Schaft, and B. Maschke. Hamiltonian discretization of boundary control systems. *Automatica*, 40(5):757–771, May 2004. http://dx.doi.org/10.1016/j.automatica.2003.12.017.

[15] R. Moulla, L. Lefevre, and B. Maschke. Pseudo-spectral methods for the spatial symplectic reduction of open systems of conservation laws. *Journal of Computational Physics*, 231(4):1272–1292, 2012. https://doi.org/10.1016/j.jcp.2011.10.008.

[16] F. L. Cardoso-Ribeiro, D. Matignon, and V. Pommier-Budinger. A port-Hamiltonian model of liquid sloshing in moving containers and application to a fluid-structure system. *Journal of Fluids and Structures*, 69:402–427, February 2017. http://dx.doi.org/10.1016/j.jfluidstructs.2016.12.007.

[17] M. Seslija, A. J. van der Schaft, and J. M. Scherpen. Discrete exterior geometry approach to structure-preserving discretization of distributed-parameter port-Hamiltonian systems. *Journal of Geometry and Physics*, 62(6):1509 – 1531, 2012. https://doi.org/10.1016/j.geomphys.2012.02.006.

[18] P. Kotyczka, B. Maschke, and L. Lefèvre. Weak form of Stokes-Dirac structures and geometric discretization of port-Hamiltonian systems. *Journal of Computational Physics*, 361:442 – 476, 2018. https://doi.org/10.1016/j.jcp.2018.02.006.

[19] M. Grinfeld. *Mathematical Tools for Physicists*. John Wiley & Sons Inc, 2nd edition, jan 2015.

[20] A. Macchelli, C. Melchiorri, and L. Bassi. Port-based modelling and control of the Mindlin plate. In *Proceedings of the 44th IEEE Conference on Decision and Control*, pages 5989–5994, Dec 2005. https://doi.org/10.1109/CDC.2005.1583120.

[21] M. Schöberl and K. Schlacher. Variational Principles for Different Representations of Lagrangian and Hamiltonian Systems. In Hans Irschik, Alexander Belyaev, and Michael Krommer, editors, *Dynamics and Control of Advanced Structures and Machines*, pages 65–73. Springer International Publishing, 2017. https://doi.org/10.1007/978-3-319-43080-5_7.

[22] F. L. Cardoso-Ribeiro, D. Matignon, and L. Lefèvre. A structure-preserving partitioned finite element method for the 2d wave equation. In *6th IFAC Workshop on Lagrangian and Hamiltonian Methods for Nonlinear Control*, pages 1–6, Valparaíso, CL, 2018. http://oatao.univ-toulouse.fr/19965.

[23] A. J. van der Schaft. Port-Hamiltonian differential-algebraic systems. In Achim Ilchmann and Timo Reis, editors, *Surveys in Differential-Algebraic Equations I*, pages 173–226. Springer Berlin Heidelberg, Berlin, Heidelberg, 2013. https://doi.org/10.1007/978-3-642-34928-7_5.

[24] C. Beattie, V. Mehrmann, H. Xu, and H. Zwart. Linear port-Hamiltonian descriptor systems. *Mathematics of Control, Signals, and Systems*, 30(4):17, 2018. https://link.springer.com/article/10.1007%2Fs00498-018-0223-3.

[25] A. Logg, K. A. Mardal, G. N. Wells, et al. *Automated Solution of Differential Equations by the Finite Element Method*. Springer, 2012. https://doi.org/10.1007/978-3-642-23099-8.

[26] D. Tong, W. Zhou, Y. Gao, C. Ji, and H. Su. H^∞ model reduction for port-controlled Hamiltonian systems. *Applied Mathematical Modelling*, 37(5):2727 – 2736, 2013. https://doi.org/10.1016/j.apm.2012.06.031.

[27] H. Egger, T. Kugler, B. Liljegren-Sailer, N. Marheineke, and V. Mehrmann. On structure-preserving model reduction for damped wave propagation in transport networks. *SIAM Journal on Scientific Computing*, 40(1):A331–A365, 2018. https://doi.org/10.1137/17M1125303.

[28] T. J. Courant. Dirac manifolds. *Transactions of the American Mathematical Society*, 319(2):631–661, 1990.

[29] A. Macchelli, A. J. van der Schaft, and C. Melchiorri. Port Hamiltonian formulation of infinite dimensional systems I. Modeling. In *Proceedings of the IEEE Conference on Decision and Control*, volume 4, pages 3762 – 3767. IEEE, 01 2005. https://doi.org/10.1109/CDC.2004.1429324.

[30] M. Renardy and R. C. Rogers. *An Introduction to Partial Differential Equations*. Number 13 in Texts in Applied Mathematics. Springer-Verlag New York, 2 edition, 2004.

[31] A. Macchelli and C. Melchiorri. Modeling and control of the Timoshenko beam. The distributed port Hamiltonian approach. *SIAM Journal on Control and Optimization*, 43(2):743–767, 2004. https://doi.org/10.1137/S0363012903429530.

[32] R. D. Mindlin. Influence of Rotatory Inertia and shear on Flexural Motions of Isotropic Elastic Plates. *Journal of Applied Mechanics*, 18:31–38, March 1951.

[33] D. N. Arnold and R. Winther. Mixed finite elements for elasticity. *Numerische Mathematik*, 92(3):401–419, Sep 2002. https://doi.org/10.1007/s002110100348.

[34] D.J. Dawe and O.L. Roufaeil. Rayleigh-Ritz vibration analysis of Mindlin plates. *Journal of Sound and Vibration*, 69(3):345–359, 1980. https://www.sciencedirect.com/science/article/pii/0022460X80904770.

[35] H.C. Huang and E. Hinton. A nine node Lagrangian Mindlin plate element with enhanced shear interpolation. *Engineering Computations*, 1(4):369–379, 1984. https://www.emeraldinsight.com/doi/pdfplus/10.1108/eb023593.

[36] R. Durán, L. Hervella-Nieto, E. Liberman, and J. Solomin. Approximation of the vibration modes of a plate by Reissner-Mindlin equations. *Mathematics of Computation of the American Mathematical Society*, 68(228):1447–1463, 1999. https://doi.org/10.1090/S0025-5718-99-01094-7.

[37] M. Kurula and H. Zwart. Linear wave systems on n-d spatial domains. *International Journal of Control*, 88(5):1063–1077, 2015. https://www.tandfonline.com/doi/abs/10.1080/00207179.2014.993337.

[38] R. Ortega, A. J. Van Der Schaft, B. Maschke, and G. Escobar. Interconnection and damping assignment passivity-based control of port-controlled Hamiltonian systems. *Automatica*, 38(4):585–596, April 2002. http://dx.doi.org/10.1016/S0005-1098(01)00278-3.

[39] R. Ortega, A. J. Van Der Schaft, F. Castanos, and A. Astolfi. Control by interconnection and standard passivity-based control of port-Hamiltonian systems. *IEEE Transactions on Automatic Control*, 53:2527 – 2542, 01 2009. http://citeseerx.ist.psu.edu/viewdoc/download?doi=10.1.1.709.4816&rep=rep1&type=pdf.

[40] A. Macchelli, Y. Le Gorrec, H. Ramirez, and H. Zwart. On the synthesis of boundary control laws for distributed port-Hamiltonian systems. *IEEE transactions on Automatic control*, 62(4):1700–1713, 4 2017. https://ieeexplore.ieee.org/document/7524022.